

Volume 41, 1983/84, No. 9

# PHILIPS TECHNICAL REVIEW



**PHILIPS**

Philips Technical Review is published by Philips Research Laboratories, Eindhoven, The Netherlands, and is devoted to the investigations, processes and products of the laboratories and plants that form part of or cooperate with enterprises of the Philips group of companies. In the articles the associated technical problems are treated along with their physical or chemical background. The Review covers a wide range of subjects, each article being intended not only for the specialist in the subject but also for the non-specialist reader with a general technical or scientific training.

The Review appears in an English and a Dutch edition, both identical in contents. There are twelve numbers per volume, each of about 32 pages. An index is given for each volume and an index covering ten volumes appears every five volumes (the latest one was included in Volume 40, 1982).

Editors:	Dr J. W. Broer Dipl.-Phys. R. Dockhorn, Editor-in-chief Dr E. Fischmann Ir J. A. Klaassen Dr J. L. Sommerdijk Ir N. A. M. Verhoeckx Ir F. Zuurveen
Editorial assistants:	Ing. P. Post T. M. B. Schoenmakers
English edition:	D. A. E. Roberts, B.Sc., M. Inst. P., A.I.L.

© N.V. Philips' Gloeilampenfabrieken, Eindhoven, The Netherlands, 1984.  
Articles may be reproduced in whole or in part provided that the source 'Philips Technical Review' is mentioned in full; photographs and drawings for this purpose are available on request. The editors would appreciate a complimentary copy.

## OTHER PHILIPS PUBLICATIONS

### **Philips Journal of Research**

A publication in English on the research work carried out in the various Philips laboratories. Published in annual volumes of six issues each of about 100 pages, size 15½ × 23½ cm.

### **Philips Telecommunication Review**

A publication in English, dealing with the technical aspects of radio, television, radar, telephone and telegraph transmission and automatic exchanges. Published in volumes of four issues, about 40 pages per issue, size 20½ × 28½ cm.

### **Electronic Components and Applications**

A publication in English, containing articles dealing with the theory and practice of electronic components and materials. Four issues per year, about 60 pages per issue, size 21 × 29½ cm.

### **Medicamundi**

A publication in English on radiology, nuclear medicine and medical electronics. Three issues per volume, about 60 pages per issue, size 21 × 29½ cm.

---

Forthcoming issues of Philips Technical Review will include articles on:

Aspherics

Piezoelectric microbalance

Magnetic bearings

DOR with tellurium alloys

Organic-dye films for optical recording

---

## Contents

	Page
DIVAC — an experimental optical-fibre communications network . . . . .	
. . . . . J. van der Heijden	253
Porosimeter measurements on magnetic tape . . . . .	
. . . . . H. F. Huisman and C. J. F. M. Rasenberg	260
Scandium for X-ray tube anode . . . . .	267
Optical aspects of the Silicon Repeater . . . . .	S. Wittekoek 268
Scientific publications . . . . .	279

---

PHILIPS TECHNICAL REVIEW  
Philips Research Laboratories  
P.O. Box 80 000  
5600 JA Eindhoven  
The Netherlands

Subscription rate per volume fl. 80.00 or U.S. \$ 35.00  
Student's subscription fl. 32.00 or U.S. \$ 14.00  
Binder fl. 10.00 or U.S. \$ 4.00

Payment only after invoicing, please.

Printed in the Netherlands



# PHILIPS

## DIVAC — an experimental optical-fibre communications network

J. van der Heijden

*Nowadays 'optical communication' usually means the exchange of information with the aid of optical fibres. The term is also applicable, however, to visual communication by semaphore or similar methods. In France between 1793 and 1852, for example, a visual communication network designed by Claude Chappe was in use. This worked with a system of moving arms that could be viewed by telescope from distances of up to 20 km. The network eventually had 556 stations and covered a total length of 4000 km<sup>[\*1]</sup>. Although this network was very successful, it probably delayed the introduction of the electric telegraph in France by 20 years or more.*

*Today something similar is happening. The introduction of optical-fibre networks is being delayed by the presence of conventional networks that work well, although optical fibres undoubtedly have distinct advantages over conventional copper cables for many communication applications.*

*To provide a general insight into the many possibilities offered by optical-fibre networks the DIVAC project was set up (DIVAC is an acronym for the Dutch words standing for digital connection between subscriber and exchange via optical fibres). In the DIVAC project experience is being gained not only with new technologies but also with new services. The parties cooperating in the project are the Dr Neher Laboratory of the Netherlands Posts and Telegraph Service, the Delft and Eindhoven Universities of Technology, Philips' Telecommunicatie Industrie B.V. and Philips Research Laboratories.*

### Introduction

A term encountered more and more widely today is 'information society'. The thinking behind this term is that we are now experiencing a transition from an industrially oriented society to an information-oriented society. The production of goods — mainly concentrated in western countries since the industrial revolution — will, it is considered, move increasingly to the countries of the third world. (The changes in the textile industry are a particular case in point.) The western countries will then become more engaged in 'intellectual production', that is to say in generating and disseminating information and in providing the necessary tools for that purpose.

We shall not enquire here into the social and political implications to which these changes would lead.

*J. van der Heijden is with Philips Research Laboratories, Eindhoven.*

What is relevant in this context, however, is that the changes have been made possible by a number of technological developments, two of which will be mentioned here. The first is the transition from analog to digital information transmission. The second is the move towards ever-higher signal frequencies, partly brought about by the perfection of optical fibres as a medium for signal transmission<sup>[1]</sup>.

In telecommunication digital signal transmission has a number of interesting advantages. Since the sig-

[\*] G. R. M. Garratt, The early history of telegraphy, Philips Tech. Rev. 26, 268-284, 1965.

[1] A. P. Bolle, Het gebruik van glasvezelkabel in lokale telecommunicatienetten, Staatsuitgeverij, 's-Gravenhage 1982 (in Dutch).

G. Mogensen, Wide-band optical fibre local distribution systems, Opt. & Quantum Electronics 12, 353-381, 1980.

N. Bjornandersen, M. Earl, O. Holst and E. Mumford (eds), Information society — for richer for poorer, North-Holland, Amsterdam 1982.

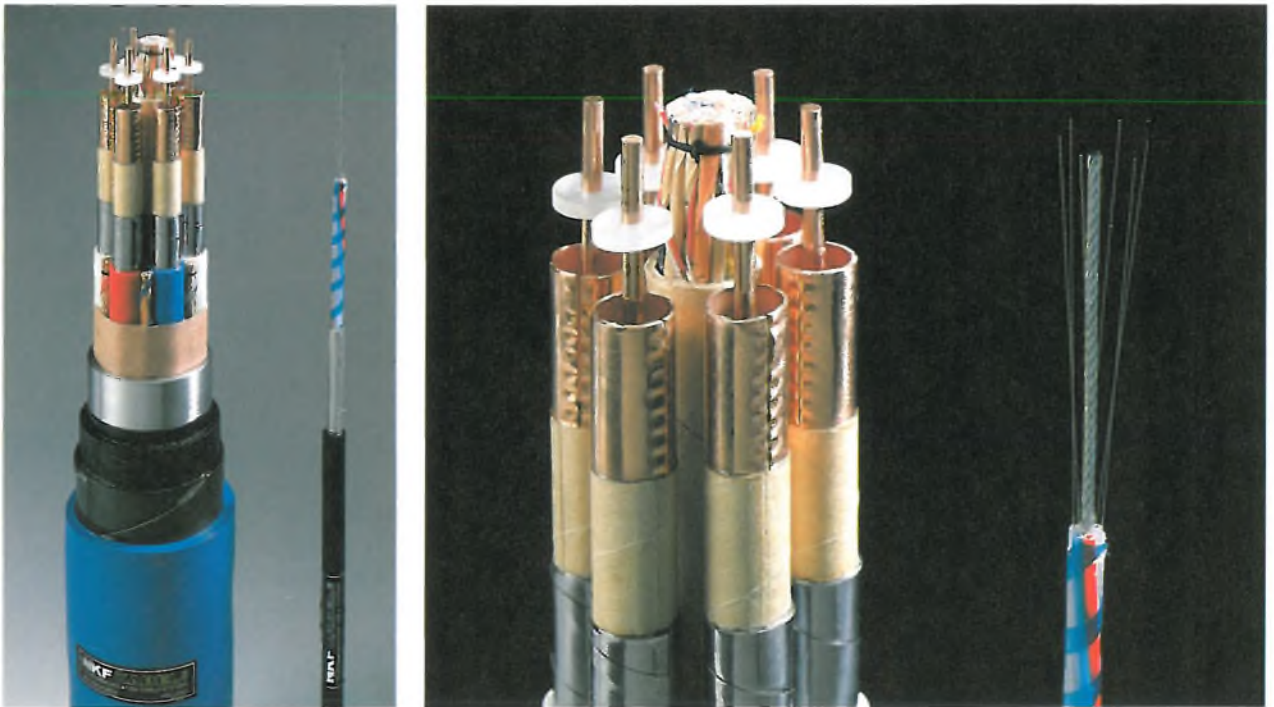


Fig. 1. Comparison of the dimensions of an optical-fibre cable and a coaxial cable, both with six cores. *Left:* general view; *right:* close-up. The copper conductors in the centre of the coaxial cable supply the signal amplifiers. The external diameter of the coaxial cable is 62 mm, the external diameter of the optical-fibre cable is 8 mm.

nals are built up from discrete voltage levels, there is less interference from the environment. A distorted signal can be restored during transmission or afterwards. Different digital signals can be 'multiplexed', so that they can be transferred as a single combined signal. The electronics required for multiplexing digital signals can be integrated more easily than the circuits required for multiplexing analog signals.

The techniques that can be used for multiplexing digital signals in optical-fibre cables are known as TDM (time-division multiplex), WDM (wavelength-division multiplex), SDM (space-division multiplex) and FDM (frequency-division multiplex). In TDM bit-groups of different signals follow one after the other in time. In WDM, signals formed from light of different 'colours' are transferred along a fibre simultaneously. In SDM a separate fibre in the cable is used for each signal. In FDM, signals of different frequency are added together. This originally analog method is used in digital technology for multiplexing signals with different bit rates, and can only be used here by virtue of coding techniques that modify the frequency spectra of the separate signals to prevent them from overlapping.

The modern optical-fibre cable for communication applications has exceptionally low attenuation — less than 1 dB per kilometre — which means that fewer repeaters are required than with coaxial cables. It also

has various other advantages. The signal is not susceptible to interference from electromagnetic fields set up by nearby cables or other sources. An optical-fibre cable is also much smaller in diameter and lighter than a coaxial cable (see *fig. 1*), so that an optical-fibre cable can often be found accommodation in an existing cable duct. Then again, the raw materials for manufacturing the glass optical fibres are widely distributed in the Earth's crust. Finally, the price of optical-fibre links is still falling, so that they can already compete economically with coaxial-cable links — especially when the costs of the repeaters are taken into account. For this reason optical-fibre cables are already in use for connections between telephone exchanges.

Many homes in Western Europe are connected to a telephone network consisting of pairs of copper wires and to coaxial-cable systems for broadcast-signal transmission via a central antenna; see *Table I*. The telephone network can be used for two-way communication, whereas the broadcasting network is intended for purely one-way communication. Limited intervention by the user is possible only in the case of Videotex (picture information is obtained here by making telephone connections).

A local optical-fibre star network, which connects an exchange directly to a number of subscribers, offers

many more possibilities than present-day communication networks. With such a network the user can obtain a wide variety of information, and he can also communicate with the exchange or with other users. The optical fibre that connects the user's home to the exchange can be made to carry different signals simultaneously through the use of multiplexing methods, and signals can be sent in both directions simultaneously by using light of different spectral composition. In local optical-fibre star networks the present communication facilities can be combined with newer services such as video telephone, pay television, video-library services, electronic shopping and electronic banking.

The concept of 'service' should be understood as a facility offered to the user via the exchange and the optical-fibre star network. A service can be a programme, a video signal, a bit stream or a stream of photons, depending on the level at which it is being considered. A hierarchical model of this kind can be assigned to any service; see *fig. 2*. The user is not interested in the technical aspects of the video signal, nor in the method of manufacture of the cable that enters his home. He is however interested in the programmes he can watch on the screen of his television set. At the various levels in the hierarchical model different persons or bodies are involved: users, television-set manufacturers, network controllers, suppliers and installers of cable networks, programme suppliers and broadcasting organizations. The rules observed by the persons and bodies involved rest to a large extent on government regulations. The advantages of integrating all existing and new services in a multiservice network are that if new systems are installed the costs are relatively low and the user can benefit from a multiplicity of services, which can be extended as required.

In countries like Canada, West Germany, France and Japan experiments on a limited scale with local

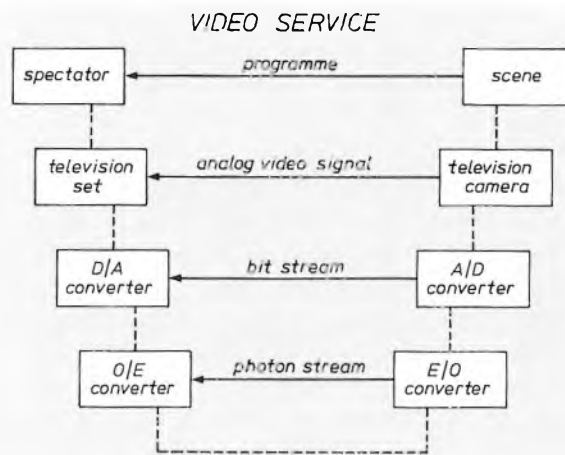


Fig. 2. Hierarchical model of a service (the video service). A/D analog/digital, D/A digital/analog, E/O electronic/optical, O/E optical/electronic.

optical-fibre networks have already been undertaken or will be carried out in the near future [4]. The object of these experiments is to gain knowledge and experience with new technologies, to assess the reaction and acceptance of the persons and bodies involved, and to encourage the enactment of appropriate legislation, rules and regulations (e.g. should the users pay for the services individually or as a package). Standards institutions can also be encouraged to consider the standardization of signals, signal processing and equipment.

An experimental local optical-fibre network has also been designed in the Netherlands. This design has resulted in a trial system that was put into operation some time ago. The project is called DIVAC (an acronym for the Dutch words standing for 'digital connection between subscriber and exchange via optical fibres'). The trial system differs from other experimental networks: all the signals are digitized, and it includes a very large number of services. To make it more readily accessible to interested parties, the system has been accommodated in a laboratory, and comprises one exchange and two 'subscribers'. The participants cooperating in the project were: Eindhoven University of Technology (audio activities), Delft University of Technology (design of the video switching network), Philips' Telecommunicatie Industrie B.V. (design of the optical units), the Dr Neher Laboratory of the Netherlands PTT (telephony), and Philips

Table I. The degree of penetration of telephony and central-antenna systems (CATV) in some countries of western Europe.

	Number of telephone connections per 100 inhabitants [2]	Number of CATV connections per 100 families [3]
Belgium	37	85
Denmark	64	61
Finland	50	44
France	46	44
Netherlands	51	65
Switzerland	73	59
United Kingdom	50	14
West Germany	46	41

[2] The world's telephones, AT&T Long Lines, Morris Plains, NJ, 1981.

[3] Cable TV communications in Western Europe, CIT Research, London 1982.

[4] J. van der Heijden, Fibre optic broadband multiservice networks, Proc. 9th ECOC (invited & post-deadline papers), Geneva 1983, 8 pp.

Research Laboratories (coding of video signals and new services). The integration of all these fields to form a complete system was undertaken by a working group in which all the partners were represented. The system was accommodated in the Geldrop Projects Centre of Philips Research Laboratories, Eindhoven. It was in operation there for more than a year, gave full technical satisfaction and attracted a great deal of interest, both at home and abroad. The system has recently been transferred to the Dr Neher Laboratory at Leidschendam to be used for demonstrations.

In the following we shall first look at the system aspects of DIVAC and at the services made available. Some of the technical features will then be discussed, and a few of the services will be examined in more detail.

### The system

As we have just seen, DIVAC is a laboratory system, with one exchange and two subscribers. The subscribers are each connected to the exchange by two optical fibres 5 km in length, partly incorporated in a twelve-core cable; see *fig. 3*. The experimental network is the simplest form of a star network with long arms, each subscriber being connected to the exchange without the intermediary of distribution stations. (A telephone network is built up in the same way; in a cable-television network, on the other hand, the subscriber is usually connected to the exchange via intermediate distribution points.) The subscribers to DIVAC can communicate with each other via the exchange, but they also have access to services offered by the exchange, originating from outside sources such as broadcasting stations or generated in the exchange itself.

Most of the signals that enter the exchange or are generated in the exchange are analog signals. The subscriber sets (which are mainly modified standard sets) usually work with analog signals. Since the optical



Fig. 3. Part of the experimental system in the laboratory. The reels of optical-fibre cable are on the left, and a demonstration display for the signal transfer can be seen on the right.

fibres in DIVAC only carry digital signals, analog-to-digital conversions and vice versa are required. In addition to these conversions the signals on the way from exchange to subscriber have to undergo electronic/optical and optical/electronic conversions, and may also have to pass through switching networks. The various possible successive operations are summarized in *Table II*.

Because of the general lack of standardization in digital signal processing, we had to design most of the signal-processing equipment for DIVAC ourselves. It is therefore rather bulky and expensive. Standardization and the use of integrated circuits should make future equipment less costly and more compact.

### Services

The following services are available for users of DIVAC:

- Distribution of audio signals. The subscriber receives 31 stereo signals simultaneously with the appropriate station and programme identifications (SPI) [5]. The definition of the audio signals in DIVAC is sufficient to give 'Compact Disc' quality for the subscriber's audio reproduction.
- Telephony. The subscriber has four telephone channels available. These signals can be fed to a 'dataphone', which is a combination of a loudspeaking telephone and a data terminal. It can be used at the same time for telephone calls and data transmission. For example, 'electronic shopping' with the dataphone

Table II. Possible successive operations on the signals in DIVAC.

analog/digital conversion	} in the exchange
switching	
electronic multiplexing (TDM and/or FDM)	
electronic/optical conversion	
optical multiplexing (WDM)	
optical demultiplexing	} at the subscriber's home
optical/electronic conversion	
electronic demultiplexing	
switching	
digital/analog conversion	

can be followed by 'electronic payment'. It is also possible to receive 'electronic mail', an 'electronic newspaper' or an 'electronic telephone directory'.

- Distribution of video signals. Selection television is used in DIVAC: the subscriber can operate a switching network via a control signal on a telephone channel to select the two video signals that he can receive simultaneously. When the system specification for DIVAC was adopted in 1981, the available bandwidth allowed the transmission of only one video signal per colour in an optical fibre. With the improved quality of fibres it would now be possible to transmit several

of being used as a 'video baby alarm'. DIVAC also includes a connection to the electronic document-handling system MEGADOC [7], which uses digital optical recording (DOR) discs. It is also possible to send in personal video recordings for local television.

**Some technical aspects**

The fibres used for the transmission of optical signals are glass graded-index fibres with a core diameter of 50 μm and an outside diameter of 125 μm. The two fibres per subscriber transmit light at wavelengths of

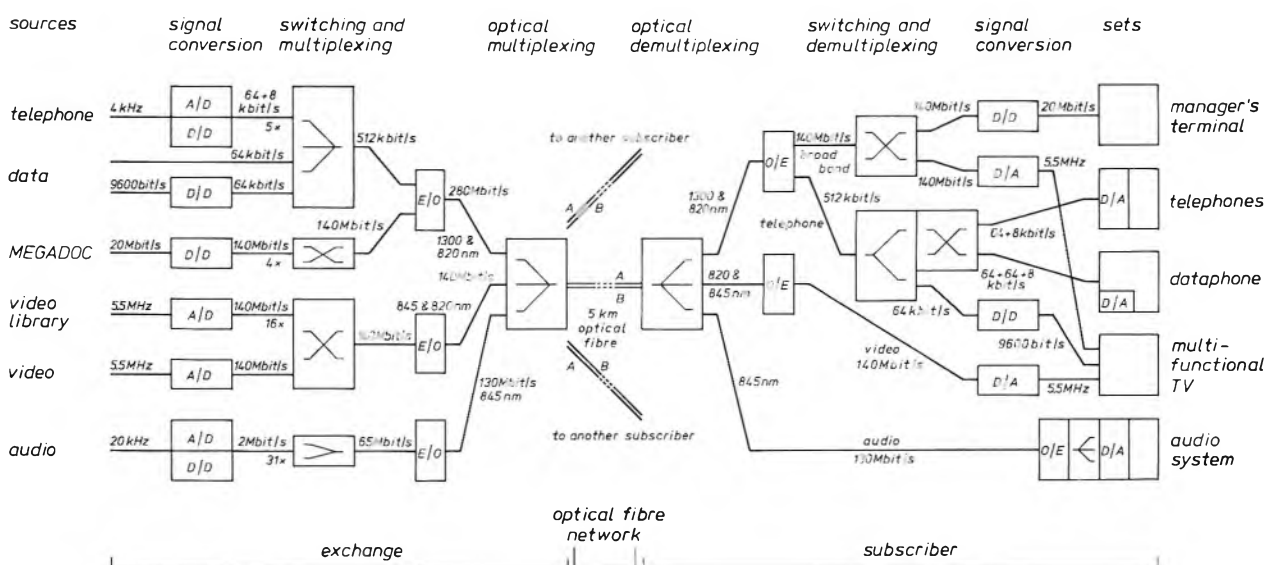


Fig. 4. Block diagram of the laboratory system. The signal sources in the exchange are shown on the left, the user sets are shown on the right. The signal operations, running from left to right, are summarized in Table II. D/D indicates conversions of digital signals into differently defined digital signals (e.g. for bit rate); see also the caption to fig. 2. The distribution of the electronic signals among the optical signals is as shown in Table III. The bandwidths of analog signals and the bit rates of digital signals are indicated beside the appropriate connecting lines, as are also the light wavelengths of the optical signals. The equipment for processing the signals at the user end is contained in a connection box, which can be made more compact in future by using special integrated circuits.

video signals per colour by means of TDM. Another reason for using selection television is that some video services are only individually available. For instance, in addition to seven broadcast video channels and one channel for local television the user also has a video-library channel available. There are also two channels for pay television and a further three channels for test signals. The video library in the DIVAC laboratory system offers a choice from a total of 150 feature films, children's programmes and musicals, together with encyclopaedic information and interactive study courses.

- Broadband services. The broadband services provided include the video telephone, with which the subscriber can send and receive image and sound signals simultaneously [6], and surveillance television, capable

820, 845 and 1300 nm, in wavelength multiplex. (In the present state of the art the number of wavelengths per fibre could be larger and one fibre per subscriber would be sufficient.) Table III indicates how the signals for the various services are distributed among the two fibres and the three wavelengths. Fig. 4 shows a block diagram of the DIVAC trial system, giving the bit rates and bandwidths of the various signals.

[5] G. C. M. Gielis, J. B. H. Peek and J. M. Schmidt, Station and programme identification in FM sound broadcasting, Philips Tech. Rev. 39, 216-225, 1980.  
 [6] Some general aspects of the video telephone are discussed in the introduction to: E. A. Aagaard, P. M. van de Avoort and F. W. de Vrijer, An experimental video-telephone system, Philips Tech. Rev. 36, 85-92, 1976.  
 [7] J. A. de Vos, Megadoc, a modular system for electronic document handling, Philips Tech. Rev. 39, 329-343, 1980.

All of the video signals except two are digitized by means of a one-bit/two-bit line-coding operation<sup>[8]</sup>, resulting in signals at 140 Mbit/s. For comparison, one of the two remaining signals is digitized by pulse-code modulation (PCM), with a sampling rate of 14 MHz, and eight bits and two added bits per sample. After a five-bit/six-bit line-coding operation, with the object of removing the direct-voltage component from the signal, a signal is obtained with a bit rate of 168 Mbit/s. The other remaining signal is first frequency-modulated with a 22-MHz carrier and a frequency deviation of 11 MHz, and is then amplitude-limited ('clipped FM')<sup>[9]</sup>.

The digitized signal of the broadband services (starting from the source 'MEGADOC' in fig. 4) has a bit rate of 140 Mbit/s. After a one-bit/two-bit line-coding operation the resultant bit rate is 280 Mbit/s. The coding removes the low-frequency components, so that the frequency spectrum of the broadband-services signal supplements that of the telephone signal, and both signals can be combined by frequency multiplexing; see Table III. The digitized telephone signal consists of a multiplex (TDM) of four signals for digital speech or for data transmission, and of the control signal that operates the switching matrices for the video signals and the broadband services. The resulting bit rate of the narrowband telephone signal is 384 kbit/s. After a six-bit/eight-bit line-coding operation a bit rate of 512 kbit/s is obtained with no high-frequency components. The narrowband and broadband signals are added together at the transmitting end and are separated by filters at the receiving end.

Each of the analog signals of the 31 stereo-audio signals is sampled at a rate of 64 kHz. With 12 or 14 bits per sample this results in a PCM signal. Bits for station and programme identification are then added to each signal. Multiplexing (TDM) of the 31 signals results in a bit rate of 65 Mbit/s, from which, after a one-bit/two-bit line-coding operation, a signal with a bit rate of 130 Mbit/s is obtained.

**Table III.** Distribution of the various optical signals among the wavelengths and fibres A and B, with the corresponding bit rates.

Optical fibre	Wavelength [nm]	Direction		Service	Bit rate [Mbit/s]
		exchange ↓ subscriber	subscriber ↓ exchange		
A	820	×		telephone	0.512
A	820	×		broadband	280
A	1300		×	telephone	0.512
A	1300		×	broadband	280
A	845	×		audio	130
B	820	×		video 1	140
B	845	×		video 2	140



**Fig. 5.** The telephone adapted for DIVAC, with keys for abbreviated dialling, automatic redialling, and for cancelling an incorrect digit (R). It has a small screen for displaying a dialled number or a caller's number.



**Fig. 6.** The manager's terminal. This can be used to connect the user to the MEGADOC system and to show stored documents on a screen. The manager's terminal can be extended to include other functions such as electronic mail and access to data bases.

### Some examples of services

The telephone modified for DIVAC is shown in fig. 5. It has a small display of 32 characters in two lines. The keyboard contains extra keys for new functions such as 'abbreviated dialling' and 'automatic redialling'.

Fig. 6 shows the 'manager's terminal'. This terminal can be used to connect the user to the MEGADOC system and to display documents on a high-resolution screen. Document retrieval requires the high bit rate of 20 Mbit/s. In the trial configuration of DIVAC the manager's terminal is confined to the MEGADOC

[8] E. Roza, An optical 1-bits video link, Proc. 7th ECOC, Copenhagen 1981, 4 pp.

[9] The various modulation techniques and some coding methods are described by F. W. de Vrijer, Modulation, Philips Tech. Rev. 36, 305-362, 1976.

facility, but in a practical situation other functions may be added such as electronic mail and access to data bases.

The screen of the 'multifunctional' television set, which can be used for a wide variety of video facilities, is shown in *fig. 7a* and *b*. The first figure shows the picture that the user receives as soon as he switches on the set. From this 'menu' he can select entertainment, communication or education, using his remote-control unit. If, for example, 'video library' is selected, a connection is made to the computer of the electronic video library and the picture shown in *fig. 7b* appears on the screen. The computer at the same time records the charge for the use of the video library. Selections from successive menus can give feature films, interactive courses, children's programmes or subjects from a video encyclopaedia. The information is stored on LaserVision video discs. The 'juke box' that retrieves these discs and puts them on a LaserVision player is shown in *fig. 8*. The computer controls this



a



b

Fig. 7. The screen of the multifunctional television set, a) when the set is switched on, b) after the user has selected 'video library'. The services can be selected using the TV remote control unit.



Fig. 8. The 'juke box' forming part of the video library in the exchange. The juke box consists of modules, each containing a LaserVision video player, a storage rack for fifty LaserVision discs and a retrieval and transport system. The mechanical system is arranged so that a player can also receive discs from other modules. The entire system is controlled by the computer of the video library.

juke box and also controls the transfer of the information on the disc to the user requesting it. The computer can also keep a record of such requests. This record can be used for combining requests so that the same information can be sent simultaneously to more than one user; the subscriber charges can be arranged to encourage this more efficient mode of operation.

**Summary.** The DIVAC project has resulted in an experimental optical-fibre communications network, which connects an exchange with two 'subscribers'. Five organizations have participated in this trial project, with the object of gaining experience with new technologies and assessing the reactions of potential users and bodies. Various digital signals, for telephony, audio, video and broadband services can be carried simultaneously and in two directions by means of TDM, WDM and FDM on a pair of optical fibres for each subscriber. The various services made available include selection television. The subscriber uses this to operate a switching network to select the required service: broadcast television, local television, a video library or pay television. The video library contains a collection of LaserVision discs, and has a control computer, a number of LaserVision players and a mechanical retrieval and transport system.

## Porosimeter measurements on magnetic tape

H. F. Huisman and C. J. F. M. Rasenberg

---

*To record half an hour of music with his Telegraphone in 1898 Valdemar Poulsen required nearly 4 km of piano wire. Today this can be done with about 85 m of thin magnetic tape, which takes up very much less space. The high quality demanded of a magnetic tape requires a complicated manufacturing process, conducted entirely in clean-room conditions. To determine the correct design data and for supervising the production process advanced analytical methods are necessary. In one such method used in the PDMagnetics magnetic-tape factory (PDMagnetics is a Du Pont-Philips joint venture), the porosity of the magnetic lacquer layer is measured with an extremely sensitive mercury porosimeter.*

---

### Introduction

Magnetic tape plays an important part in modern society. After the development of the Compact Cassette for sound recording at the end of the sixties<sup>[1]</sup>, and its international standardization, audio magnetic tape 3.81 mm wide is now produced in large quantities throughout the world. As a consequence of the growing popularity of the video cassette recorder there is a considerable demand for 12.7-mm video magnetic tape. Because of its high information density video tape has to meet a much tighter specification than audio tape.

In the design and manufacture of magnetic tape the aim is to store as much information on the tape as possible within the wound volume. This can be achieved by applying a carefully distributed and structured magnetic material to a very thin carrier. Thus, modern magnetic tape consists of a polyester base material 7  $\mu\text{m}$  to 25  $\mu\text{m}$  thick coated with a thin layer of lacquer; the coating consists of a polymer binder with  $\gamma\text{-Fe}_2\text{O}_3$ ,  $\text{CrO}_2$  or metal-powder particles embedded in it. The particles have a length of about 0.5  $\mu\text{m}$  and a diameter of about 0.1  $\mu\text{m}$ . The ratio of particle volume to coating volume must be as high as possible because of the electromagnetic requirements for the tape.

During the manufacturing process a suspension of magnetic particles in a binder solution is poured on to the base material. (By analogy with paint manufacture the magnetic particles are usually referred to as 'pigment'.) Before the solvent has entirely evaporated, the needle-shaped particles are oriented in the longitudinal direction of the tape by means of a magnetic field. After this operation the particles must stack in such a way that the binder with the embedded particles takes up the minimum volume. The ratio of particles to coating in this stacking arrangement, on condition that the space between the particles is entirely filled with binder, is called the critical pigment-volume concentration (CPVC).

The suspension of magnetic particles in the binder solution is not stable. The mobility of the particles is increased by adding dispersing agents or stabilizers<sup>[2]</sup> and stirring the solution. Magnetic forces cause the formation of clusters of needle-shaped particles, which are found in the lacquer coating on the tape; see *fig. 1*.

The concentration of particles in the magnetic layer must of course be as high as possible, but if the concentration is too high interstices form between the clusters, and pores form in the actual clusters. In practice a concentration slightly above the critical pigment-volume concentration is found to give the best

---

*Dr H. F. Huisman and Ing. C. J. F. M. Rasenberg are with PDMagnetics, Oosterhout.*

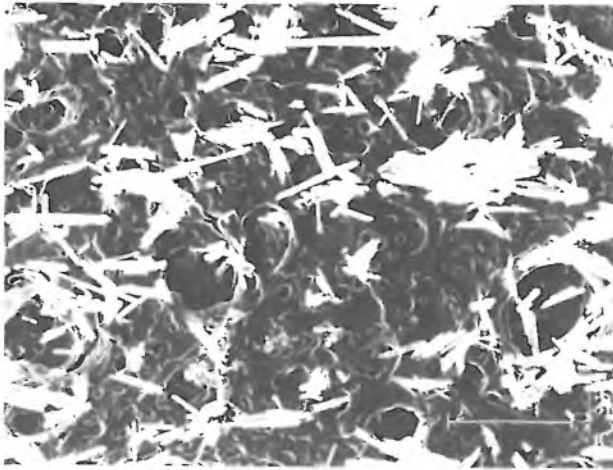


Fig. 1. Transmission electron micrograph of magnetic tape etched with hydrochloric acid. The white areas are clusters of  $\text{CrO}_2$  particles. The black areas give the locations of the clusters of  $\text{Fe}_2\text{O}_3$  particles; these particles were removed on etching. The  $\text{Fe}_2\text{O}_3/\text{CrO}_2$  volume ratio was 95:5. The length of the line in the photograph corresponds to  $1\ \mu\text{m}$  in the sample.

results. After the drying process the interstices and pores are compressed and to some extent completely closed by calendering the tape, which consists in passing it between a number of extremely smooth rollers under pressure. The calendering improves the surface quality of the tape, so that there is less wear as the tape travels past the heads and the guide pins in the recorder. This improved surface quality also reduces the average distance between tape and head, so that reproduction of the higher frequencies is also improved.

If the tape is not calendered, interstices and pores caused by exceeding the critical pigment-volume concentration cause tape wear and shorten the useful life of the tape. Irregularities in the tape due to an excessively high local concentration of pores may even cause loss of contact between tape and head, resulting in a 'drop-out', i.e. a brief loss of information. In some cases, on the other hand, pores in the tape are desirable. In video tape, for example, pores may be created by certain additives at a fairly critical pigment concentration. In the cured coating these pores are partly filled by lubricant that was dispersed in the liquid lacquer. During use the lubricant diffuses to the tape surface and gradually becomes available to improve the sliding of the tape. These deliberately introduced pores are smaller in cross-section than the unwanted pores. It is obviously very important to keep the number of pores and their dimensions under careful control during the manufacturing process.

A method of measuring the porosity of materials was described as long ago as 1945 [3]. In this method the materials are first immersed in mercury, the pres-

sure is then increased and the change in the mercury volume is measured. This is the principle of the type 200 Carlo Erba mercury porosimeter, which we have used. Since this instrument was designed for measuring the porosity of powders, and since only small quantities of material are used in measurements on magnetic tape, it was necessary to improve the sensitivity of the mercury porosimeter. We therefore modified the instrument to make it ten times more sensitive. The results of measurements with the modified porosimeter can be used to calculate the total number of pores and their dimensions.

In the rest of the article we shall first consider the construction of the porosimeter and the interpretation of the curves obtained. We shall then show how the porosity information is obtained from these curves, and finally we shall discuss some actual measurements.

#### The mercury porosimeter and the penetration curve

The principle of the mercury porosimeter is illustrated in the diagram of *fig. 2*. The sample — a rolled-up piece of magnetic tape — is introduced into a quartz-glass dilatometer with a calibrated neck. The dilatometer is evacuated and filled with mercury. The dilatometer is then placed in a pressure vessel filled with ethanol, in which the pressure is gradually raised to about 2000 bars. The mercury is forced into the interstices and pores of the sample, so that the total volume of mercury and sample is reduced, producing a drop in the mercury level. The compression acting on the dilatometer decreases its internal volume. This effect alone would cause an increase in the mercury level. In addition the mercury and the sample are compressed.

The different changes in volume result in a fall in the mercury level in the neck of the dilatometer. This fall is measured with a metal pin. After a certain pressure increase the pin is screwed downwards until it touches the surface of the mercury. This is detected by a sharp decrease in the electrical resistance between the pin and a contact in the base of the dilatometer. The rotation of a disc attached to the pin gives a measure of the mercury level in the neck. (The accurate determination of this angular displacement by means of a light source with a photocell and a hundred slits

[1] P. van der Lely and G. Missriegler, Audio tape cassettes, Philips Tech. Rev. 31, 77-92, 1970.

[2] G. Frens, H. F. Huisman, J. K. Vondeling and K. M. van der Waarde, Suspension technology, Philips Tech. Rev. 36, 264-270, 1976.

[3] H. L. Ritter and L. C. Drake, Pore-size distribution in porous materials, Ind. & Eng. Chem. Analyt. Edn 17, 782-786, 1945; L. C. Drake and H. L. Ritter, Macropore-size distribution in some typical porous substances, *ibid.*, 787-791.

arranged around the circumference of the disc is one of the modifications we have introduced.)

When tape with initially open pores is measured in the porosimeter the result shown by curve *A* in *fig. 3a* is obtained. The linear parts 1, 2, 3 and 4 of this curve each belong to a different part of the compression and penetration process. Part 1 of the curve, almost coincident with the  $-\Delta V$  axis, corresponds to the filling of the spaces between the turns of the tape. Part 2 corresponds to the compression of the tape, without the mercury penetrating into the pores. Part 3 corresponds to the penetration of mercury into the pores. Part 4 shows the change in the volume of the mercury, the dilatometer and the sample with the filled pores.

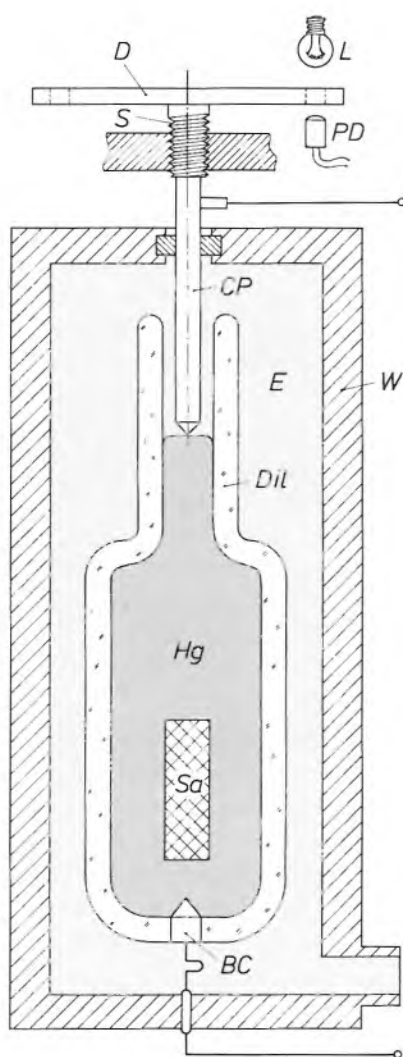


**Fig. 2.** Diagram of cross-section of part of the interior of the mercury porosimeter. *Sa* sample. *Hg* mercury. *Dil* quartz-glass dilatometer. *E* ethanol, whose pressure is slowly increased during the measurement. *W* pressure vessel. *CP* contact pin. *BC* contact in base of dilatometer. *S* screw with 1 mm pitch. *D* disc containing 100 slits evenly spaced around the circumference. After each increase in pressure, *S* is screwed downwards until the electrical resistance measured between *CP* and *BC* has fallen almost to zero. The change in the volume of *Hg* is obtained from the rotation of *D*. This is measured by counting the number of slits in *D* that have passed the light source *L* and the photodiode *PD*.

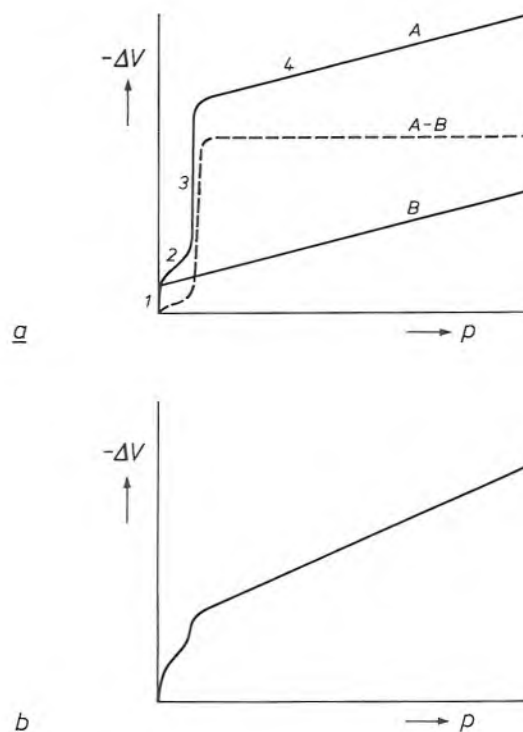


**Fig. 3.** The change  $-\Delta V$  in the volume of the mercury (*Hg* in *fig. 2*) as a function of the pressure *p*. *a*) For magnetic tape with initially open pores. *A* measured curve: 1 filling the spaces between the rolled-up tape, 2 compression of the tape, 3 penetration of mercury into the pores, 4 remaining change in volume of mercury, dilatometer and sample (with filled pores). *B* correction line to allow for the changes of volume corresponding to lines 1 and 4. *A - B* penetration curve, the difference between curve *A* and correction line *B*. *b*) Curve from measurements on tape in which the pores have been closed by calendering.

Since we are not interested in the changes of volume corresponding to 1 and 4, we correct the measured curve *A* by using line *B*, which represents these changes in volume alone. The result is the curve *A - B*, which we shall refer to as the 'penetration curve'. For this correction and other operations on the result of the measurement, as described below, the instrument is connected to a Philips PM4410 microcomputer, which also controls the measuring process<sup>[4]</sup>, see *fig. 4*. During this process the pressure is continuously increased by certain amounts — the size of step can be adjusted — and commands are given to measure the change in volume. The pairs of points (*p*,  $\Delta V$ ) thus obtained provide the result, which is displayed on a Philips PM8151 digital plotter.

When magnetic tape whose pores have been closed by calendering is measured with this system, a different curve from curve *A* is obtained. Part 3 is then very small, but part 4 has a larger slope because of the increase in the compressibility of the sample (see *fig. 3b*). It is therefore possible to see from the shape of the measured curve how the tape has been calendered.

### Calculation of some pore parameters

Information on the pores in the magnetic tape can be deduced from the shape of the penetration curve ( $A - B$  in fig. 3a) if a simplified pore geometry is assumed. We shall assume that the pores do not widen with depth (no 'ink-bottle' pores) and are cylindrical in shape.

It is known that the surface of most solids is not wetted by a drop of mercury. This implies that the contact angle  $\theta$  of the mercury droplet is in most cases

force  $F_1 (= -2\pi r\sigma \cos \theta)$ , due to the surface tension  $\sigma$  (in N/m), has to be overcome by the force  $F_2 (= \pi r^2 p)$ , due to the pressure in the mercury; see fig. 5b. From this we have the Washburn relation

$$p = - \frac{2\sigma \cos \theta}{r}. \quad (1)$$

This equation shows that the pressure required for the penetration of mercury into the pore is related to the equivalent pore radius.

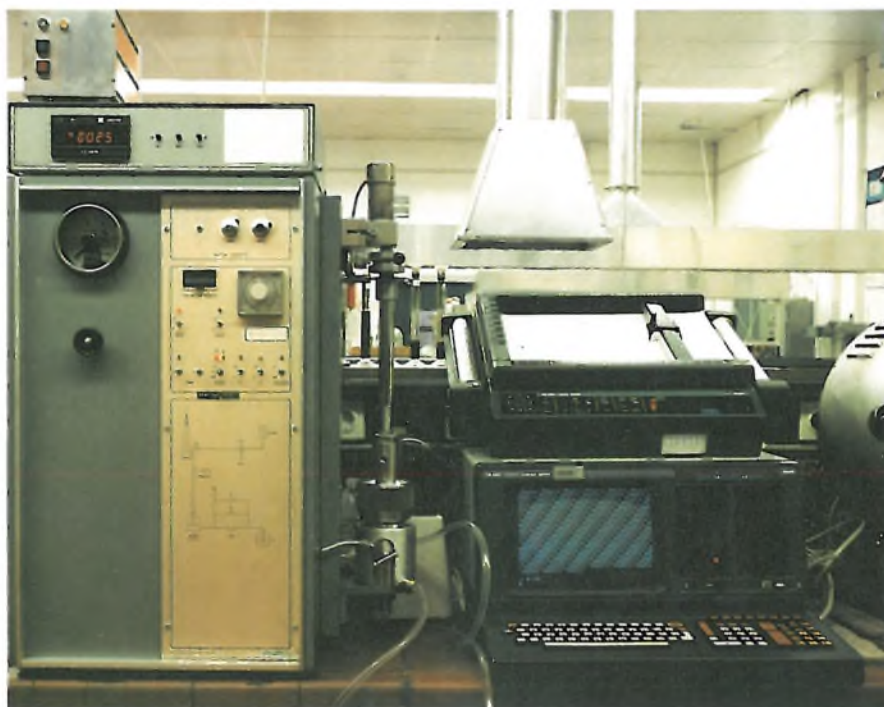


Fig. 4. Photograph of the complete measurement system. Left, the Carlo Erba type 200 mercury porosimeter; top right, Philips PM8151 digital plotter; bottom right, Philips PM4410 micro-computer, which controls the measuring process and calculates the results.

greater than  $90^\circ$  (see fig. 5a). For mercury and the coating of magnetic tape the contact angle is between  $130^\circ$  and  $160^\circ$ . The consequence is that mercury will not spontaneously penetrate into an evacuated pore of the tape, but that a certain pressure  $p$  is required in the mercury. The relation between  $p$  and the radius for a cylindrical pore has been calculated by E. W. Washburn<sup>[5]</sup>. The radius  $r$  of this simplified pore will be referred to here as the 'equivalent pore radius'. The

With the aid of fig. 5b we can also derive the expression given by H. M. Rootare and C. F. Prenzlou for the total theoretical surface area of all the pores<sup>[6]</sup>. The work that must be performed to force the mercury completely into the pores is equal to  $\int_0^{V_m} p dV$ , where  $V_m$  is the total pore volume;  $V_m$  is therefore equal to the change in the volume of the mercury during the penetration process. This work must be equal to the work performed by the force  $F_1$ , integrated over all the pores. Hence

$$\int_0^L (-2\pi r\sigma \cos \theta) dl = \int_0^{V_m} p dV,$$

where  $l$  is the displacement of the mercury in the direc-

[4] H. F. Huisman, C. J. F. M. Rasenberg and J. A. van Winsum, An improved mercury porosimetry apparatus — some magnetic tape applications, *Powder Technol.* 36, 203-213, 1983.

[5] E. W. Washburn, The dynamics of capillary flow, *Phys. Rev.* 17, 273-283, 1921.

[6] H. M. Rootare and C. F. Prenzlou, Surface areas from mercury porosimeter measurements, *J. Phys. Chem.* 71, 2733-2736, 1967.

tion of the pore and  $L$  is the total length of all the pores. Putting  $\int_0^L 2\pi r dl$  equal to the total pore area  $S$  (and hence neglecting the 'bottom' of the pore), we find

$$S = \frac{-1}{\sigma \cos \theta} \int_0^{V_m} p dV, \quad (2)$$

where  $\int_0^{V_m} p dV$  corresponds to the hatched area in fig. 6a, so that the total pore area can be calculated from the penetration curve.

We are also interested in the distribution of the volume of the pores as a function of the pore radius, expressed as  $dV/dr$ . The relative pore-volume distribution is equal to  $dV/(V_0 dr)$ , where  $V_0$  is the volume of the sample. With the aid of equation (1) this can be rewritten as

$$\frac{1}{V_0} \frac{dV}{dr} = \frac{p^2}{2\sigma V_0 \cos \theta} \frac{dV}{dp}. \quad (3)$$

In the part of the penetration curve that corresponds

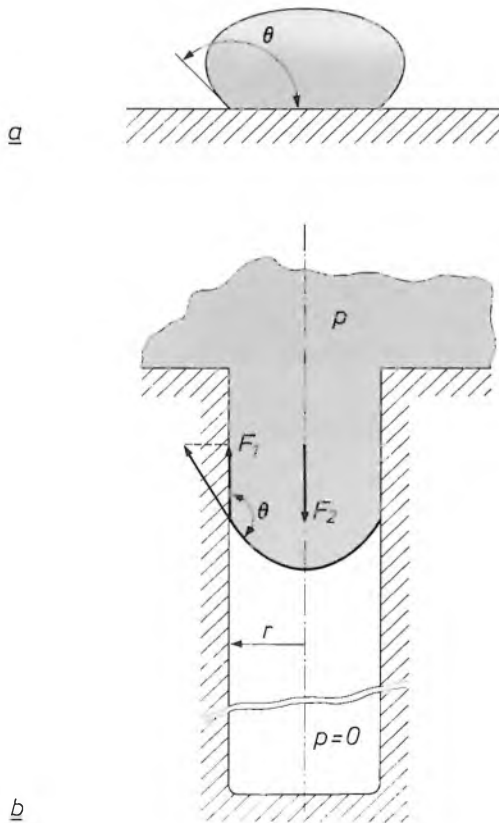


Fig. 5. a) A drop of mercury on the surface of a solid.  $\theta$  contact angle. Since  $\theta$  is greater than  $90^\circ$ , the surface of the mercury is not wetted. b) Penetration of mercury into a cylindrical pore of radius  $r$ . Since  $\theta > 90^\circ$ , the mercury must have a pressure  $p$ .  $F_1$  resultant of the forces acting on the mercury surface at the pore wall and due to the surface tension. (In reality the operating line of  $F_1$  coincides with the centre-line of the pore.)  $F_2$  downward force in the pore cross-section, due to the pressure  $p$  in the mercury. For the mercury to penetrate into the pore the condition  $F_2 > F_1$  must be fulfilled.

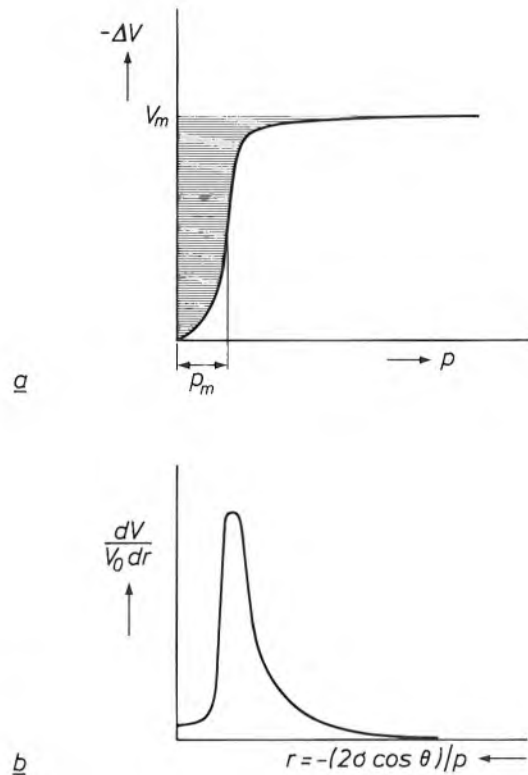


Fig. 6. a) Calculation of the total pore area from the penetration curve (see fig. 3a). The hatched area is a measure of the total pore area.  $V_m$  total pore volume: change in mercury volume in the porosimeter during the penetration process. b) Calculation of the relative pore-volume distribution  $dV/(V_0 dr)$ . This distribution can be found, except for a constant, by differentiation of the curve from a. The pore radius  $r = -2\sigma \cos \theta/p$  must then be plotted along the horizontal axis in the opposite direction.

to the filling of the pores, the pressure changes very little, so  $p$  may be taken equal to the mean value  $p_m$  (see fig. 6a). The required pore-volume distribution is then equal to

$$\frac{1}{V_0} \frac{dV}{dr} = \frac{p_m^2}{2\sigma V_0 \cos \theta} \frac{dV}{dp}. \quad (4)$$

The relative pore-volume distribution as a function of  $r$  can thus be obtained, except for a constant, by differentiating the penetration curve, taking  $\Delta V = V - V_0$  and using  $r = -(2\sigma \cos \theta)/p$  from equation (1); see fig. 6b. For normal values of the surface tension and the contact angle,  $\sigma = 0.485 \text{ N/m}$  and  $\theta = 140^\circ$ , the pressure range from 1 to 2000 bars corresponds to a change in the equivalent pore radius of  $7.5 \mu\text{m}$  to  $3.75 \text{ nm}$ .

Some results of measurements

Fig. 7a shows the measured relative pore-volume distribution of iron-oxide tape with a pigment concentration that is higher than the critical concentration.

The average equivalent pore radius is about 40 nm; the spread in the values of the pore radii is small. From repetitions of such measurements it was found that variation of the pigment concentration up to values far above the critical concentration caused little change in the pore-volume distribution. The total pore volume does change, of course. The equivalent pore radius thus appears to be fairly constant and only depends on the wetting and packing properties of the magnetic particles.

Fig. 7b shows the influence of the curing time of the coating on the effect of calendaring. In an incompletely cured coating the pores can easily be closed under the pressure of calendaring. On some tapes for which the curing times between the drying and calendaring were not the same, measurements were made of the pore volume per unit mass,  $V_m/M$ . It was found that after a curing time of more than a week the pore volume was still not constant. The curing of the coating is obviously a slow process. The usual method of measuring the degree of curing is to determine the remaining quantity of isocyanate hardener. This can be done by means of infrared spectrometry. This analysis is not very reliable, however, since the pigment absorbs most of the useful infrared radiation. A wet-chemical analysis is also unreliable because the lacquer layer becomes insoluble after a certain amount of curing.

A method of determining the critical pigment concentration is shown in fig. 7c. The graph gives the measured relative pore volume  $V_m/V_0$  as a function of the pigment concentration in percentage by weight. If the critical pigment concentration is exceeded, the porosity of the lacquer layer increases sharply. The critical pigment concentration is found from the intersection of the line through the measured points with the horizontal axis. This determination is much more accurate than the usual method, measuring Young's modulus of samples with different pigment concentra-

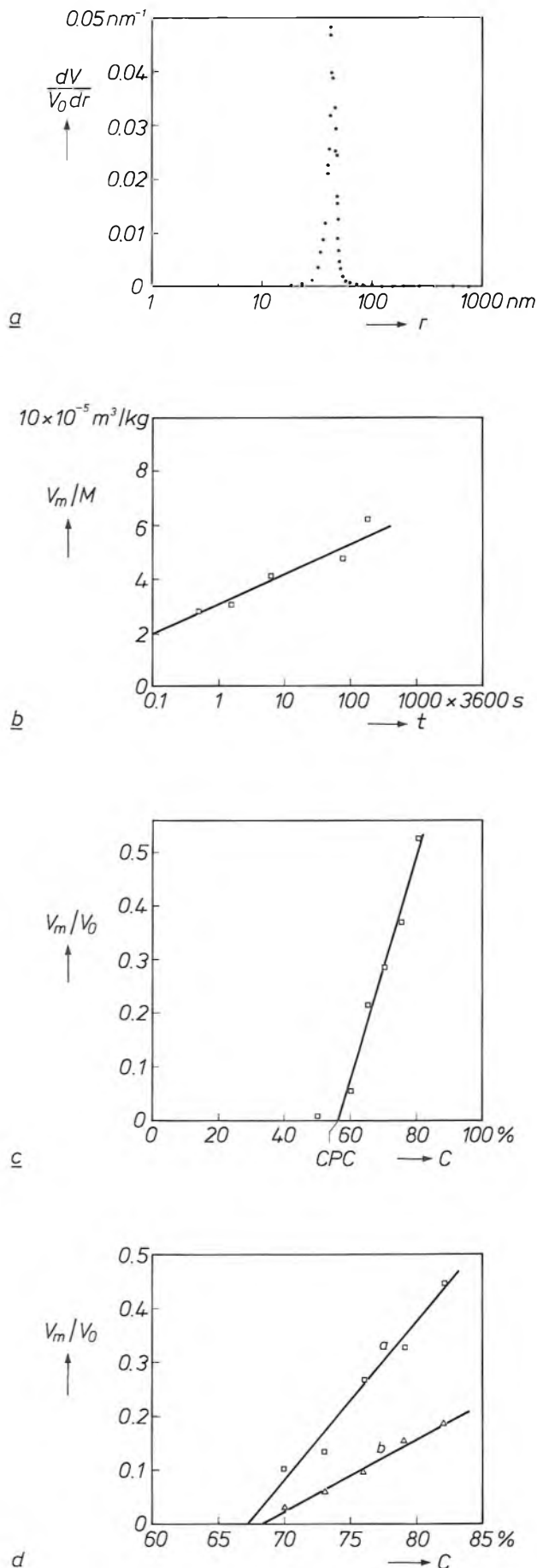


Fig. 7. Some results of measurements. a) The relative pore-volume distribution  $dV/(V_0 dr)$  as a function of pore radius  $r$ , for iron-oxide tape with a pigment concentration higher than the critical value. b) The ratio of pore volume  $V_m$  to mass  $M$  for five tape samples, as a function of the time  $t$  between drying the lacquer layer and calendaring. The time  $t$  thus determines the degree of curing of the lacquer layer. The pores in an incompletely cured layer can easily be closed by calendaring. The continuous rise of the line through the measured points shows that the layers are not completely cured at the time of calendaring. c) Determination of CPC, the critical pigment concentration, in percentage by weight. The relative pore volume  $V_m/V_0$  of a number of samples is measured and plotted as a function of the pigment concentration  $C$  in percentage by weight.  $V_0$  volume of the sample. The CPC can be found from the point of intersection between the line through the measured points and the  $C$ -axis, since the pore volume increases approximately linearly when the critical pigment concentration is exceeded. d) The same measurements on uncalendered (a) and calendered (b) metal-powder tape. In calendered tape the pores are thus partly closed and the critical pigment concentration is slightly higher.

**Table I.** Effect of calendaring on the relative pore volume and useful life of metal-powder magnetic tape with a pigment-weight concentration of 73.5%, as a result of measurements. The useful life is indicated on a relative scale with values of 1 (short) to 5 (long).

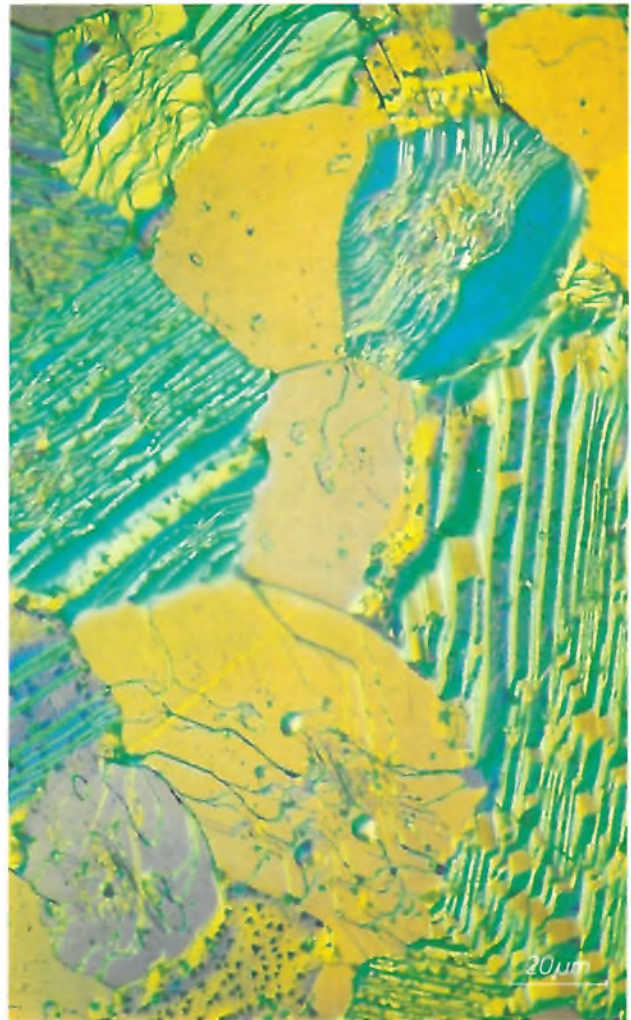
Relative pore volume (percentage)	Relative useful life	Degree of calendaring
31	1	uncalendered
18	1	lightly calendered
6	3	normally calendered
4	4-5	intensively calendered

tions. The latter method is hardly feasible for magnetic tape since the coating has to be measured without the base material. It would also be very difficult to calender unsupported layers of lacquer.

Fig. 7d shows the effect of calendaring on the total pore volume of metal-powder tape. The graph gives measured results comparable with those in fig. 7c for uncalendered (*a*) and for calendered (*b*) tape. Calendaring thus results in less porosity and, as pointed out earlier, increases the useful life of the tape. This also

appears from *Table I*, which gives the relative pore volume and relative useful life of four samples of metal-powder tape subjected to different calendaring conditions. The pilot-production proces that gave the measured results in the bottom line is now the standard method in the PDMagnetics tape factory at Oosterhout.

**Summary.** With a commercial mercury porosimeter, modified in various ways to give higher sensitivity, measurements can be made of the pore volume, the total pore area and the pore-volume distribution of magnetic tape. In calculating the results the curve giving the change in mercury volume as a function of mercury pressure has to be corrected for the compressibility of the mercury and the change in the volume of the dilatometer. The total pore area and the pore distribution are obtained by integration and differentiation of the corrected curve. From pore-volume measurements on different tape samples the critical pigment concentration can be determined. If this concentration is exceeded, pores are formed, but this negative effect can be eliminated by calendaring.

*a**b*

## Scandium for X-ray tube anode

The photomicrographs above were made during an investigation into suitable materials for the anodes of X-ray tubes for X-ray fluorescence spectrometry. They show a scandium surface after heat treatment in vacuum. Interference contrast has been used to make the crystallites in the surface clearly visible (*a*). A higher magnification (*b*) exposes the surface structure of the crystallites themselves, revealing features such as steps (right) and pits (below).

X-ray fluorescence spectrometry is a method of non-destructive testing in which a specimen is irradiated with X-rays. Absorbed X-rays can release electrons from the K or L shells of the atoms. When the sites which then become vacant are filled by other electrons,

X-ray fluorescence radiation may be emitted. The wavelength of this radiation depends on the nuclear charge of the atom, not on the chemical valence state. X-ray fluorescence can therefore be used to determine the constituent elements of a specimen. For efficient excitation the wavelength of the incident X-rays should not be much longer than that of the excited fluorescence radiation. In this respect scandium seems to be an attractive anode material. Since the wavelength is fairly long ( $\lambda_{ScK\alpha} = 0.303 \text{ nm}$ ) lighter elements (carbon to calcium) can be detected more easily than with an X-ray tube that has a chromium anode, such as the tubes commonly used in X-ray fluorescence spectrometry.

# Optical aspects of the Silicon Repeater

S. Wittekoek

---

*The Silicon Repeater, designed for the repeated projection of photomasks on a silicon wafer in the fabrication of integrated circuits in our laboratories, has been briefly described in an earlier issue of this journal<sup>[\*]</sup>. Meanwhile some substantial improvements have been made: the equipment is now faster and a larger silicon wafer can be exposed with higher resolution of details. The article shows that the Silicon Repeater owes its excellent specifications — largely determined by physical limits associated with the use of visible light — to the advanced design of the optical system.*

---

## Introduction

At the start of each process step in the manufacture of integrated circuits an intricate and highly detailed light pattern (the photomask) has to be projected on to the thin film of photosensitive lacquer (photoresist) that covers the surface of the silicon wafer. Because of the continuing developments in IC manufacture the performance required of the imaging equipment also has to show a steady improvement: photomask details are becoming smaller, IC dimensions and wafer diameters larger, and the production rates required continue to grow.

At present the method most widely used in IC manufacture is the projection of the photomask on to the wafer surface by means of visible light. The projection equipment used generally gives an actual-size image of the mask, extending over the entire surface of the wafer. This procedure has some disadvantages. The 5-inch wafers currently used require a projection lens system with a large image field, so that the numerical aperture must remain small to minimize imaging errors at the edges<sup>[1]</sup>. This small aperture limits the resolution of the objective lens. Another serious drawback of 1:1 projection is that it is virtually impossible to make the large masks required completely without faults. There are other disadvantages: departures from flatness of the wafer can cause blurring of the image, no allowance can be made for wafer deformations, and it is difficult to modify the projection equipment to suit larger wafer dimensions.

*Dr S. Wittekoek is with Philips Research Laboratories, Eindhoven.*

The wafer stepper designed at Philips Research Laboratories, which we have called the 'Silicon Repeater', does not expose the wafer in its entirety but only parts of it in steps. A photomask that contains much less information is projected on to the wafer at a fifth of full scale. After each exposure step the wafer is rapidly and accurately displaced through a distance of say 10 mm, and the next part of the wafer is then exposed. Because of the small image field the projection lens has a numerical aperture of 0.3, a high value, giving a high resolution. The objective can be refocused at each step, so that departures from flatness of the wafer need not cause blurring in the image. At every step allowance can also be made for wafer deformation during manufacture, by aligning the wafer in relation to the photomask.

The masks for the Silicon Repeater have details five times larger than those in the masks for 1:1 projection. They are therefore not so difficult to make — partly because they contain less information. Faults in the mask can sometimes be corrected or repaired. A disadvantage is that a tiny speck of dust — and this can appear even in clean-room conditions — is repeatedly projected on to the wafer and can render it useless. This problem can be solved, however, by fitting an extremely thin 'pellicle' on both sides of the mask.

---

[\*] A. G. Bouwer, G. Bouwhuis, H. F. van Heek and S. Wittekoek, The Silicon Repeater, Philips Tech. Rev. 37, 330-333, 1977.

The improved ('Mark 2') Silicon Repeater is shown in *fig. 1*. The optical system is illustrated schematically in *fig. 2* and the principal numerical data are summarized in *Table I*. The mechanical movement can thus displace the wafer through 10 mm in 0.3 s with

of interference between the incident beam and the beam reflected from the wafer surface. This has the result that the widths of linear tracks are not constant after development. The projection lens is required to have a high resolution and hence a large aperture angle



Fig. 1. The Mark 2 Silicon Repeater, an improved version of the earlier Silicon Repeater designed at Philips Research Laboratories and described in this journal [1\*]. The improved Silicon Repeater can expose sixty 4-inch silicon integrated-circuit wafers per hour.

an accuracy of  $0.1 \mu\text{m}$ . This short displacement time partly accounts for the considerable production rate of sixty exposed 4-inch wafers an hour. The exceptionally high mechanical accuracy required is achieved by using a wafer table mounted on air bearings, hydraulic servocontrol and a laser-interferometer measuring system. The details of the wafer-table control system will not be discussed in this article, which is concerned solely with the optical aspects of the equipment.

In designing the optical system of the Silicon Repeater it was necessary to satisfy a number of more or less conflicting requirements [2]. To avoid chromatic aberration in the projection the mask should ideally be exposed to monochromatic light. However, this causes intensity differences in the photoresist because

on the image side. However, a large aperture angle entails a small depth of focus, and any departure from flatness of the wafer must not cause blurring or variation in the magnification of details.

The problems indicated above have been solved in the Silicon Repeater in the following way. The mask is illuminated by a high-pressure mercury-vapour lamp of high luminous output. The radiation at *two* different wavelengths in the spectrum of this light source

[1] In one method of 1:1 projection the image errors are minimized by limiting the image field in one direction to a few millimetres. The mask and wafer are then moved through the image field together. However, the numerical aperture with this method is no larger than 0.16.

[2] S. Wittekoek, Step-and-repeat wafer imaging, *Solid State Technol.* 23, No. 6 (June), 80-84, 1980.  
R. Kramer, R. Vervoordeldonk, S. Wittekoek, R. Beem and G. van der Looij, Philips wafer stepper: characterization and processing experience, *Proc. SPIE* 334, 95-104, 1982.

is used: 405 and 436 nm, corresponding to the h and g lines respectively. With practical photoresist thicknesses between 0.7 and 1.1  $\mu\text{m}$  this method is virtually free of interference effects. A two-sided telecentric

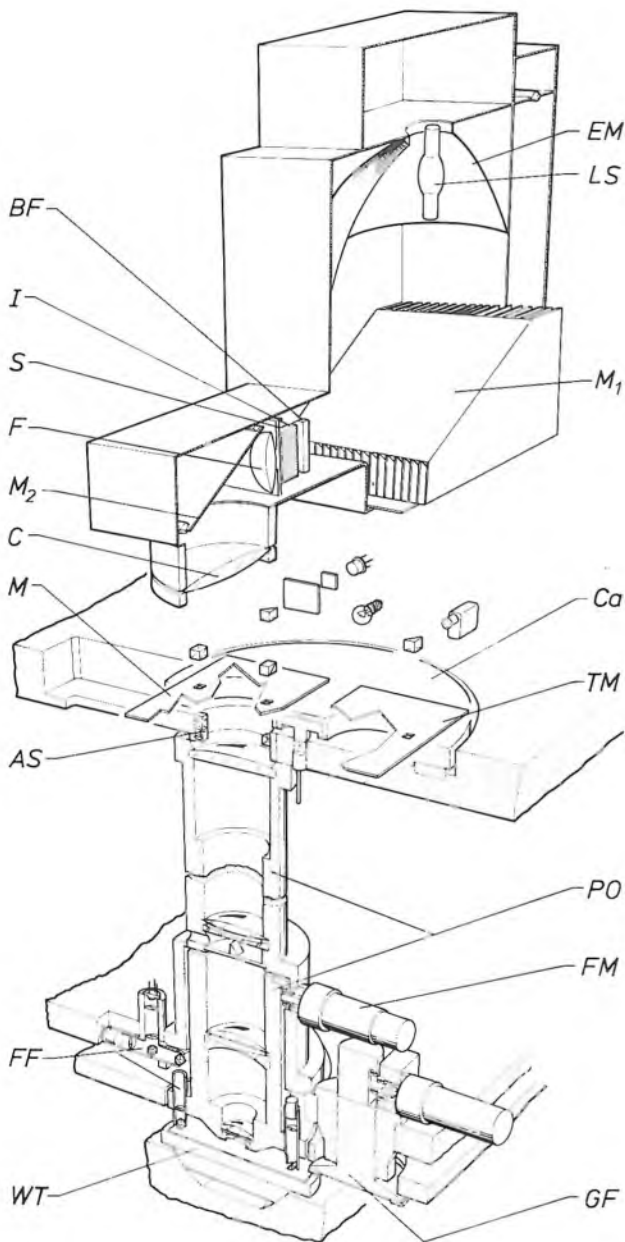


Fig. 2. Drawing of the optical system. *LS* high-pressure mercury-vapour lamp, 350 W. *EM* elliptical reflector, *M<sub>1</sub>* and *M<sub>2</sub>* flat reflectors. (*M<sub>1</sub>* is at the same time a multilayer interference filter that only reflects radiation at wavelengths below 450 nm.) *BF* bandpass filter (also a multilayer interference filter), which passes radiation of 395 to 440 nm. *S* shutter, necessary because the mercury-vapour lamp is not switched off between the projections. *F* field lens. *C* condenser. *I* optical integrator, whose operation is explained in fig. 3. *Ca* carousel for two masks; masks can be changed in 1.5 s. *M* mask. *TM* mask for test patterns. *AS* optics of alignment system. *PO* projection optics consisting of two parts. *FM* motor for displacing the lower part of *PO* for fine focusing. *FF* optical system for fine focusing. *WT* wafer table. *GF* mechanism for adjusting the upper surface of the wafer to a predetermined height (coarse focusing) and perpendicular to the optical axis. (In *WT* the spherical bearing for the angular displacement is shown but not the bearing for the vertical adjustment.)

optical system<sup>[3]</sup> has been designed for the projector. This has a numerical aperture of 0.3, and is corrected for the narrow wavelength range from 400 to 440 nm. (It is more difficult to design an optical system for a range of wavelengths than for a single wavelength.) To obtain optimum focusing the upper surface of the wafer is first positioned with a levelling mechanism for coarse focusing and angular adjustment (see fig. 2). An automatic fine-focusing system comes into operation at each projection step. The residual focusing error is less than 0.3  $\mu\text{m}$ .

The origin for the displacements is accurately determined by aligning the wafer relative to the mask in such a way that the exposures corresponding to the successive process steps are in exact register. The alignment system makes use of gratings, located both in the mask and on the wafer. The total registration error, summed vectorially for the *x*- and *y*-directions, does not exceed 0.25  $\mu\text{m}$ .

We now go on to consider first the exposure of the mask and wafer, and the projection of the mask on to the wafer. We shall then consider the alignment of the wafer in relation to the mask.

Table I. Some numerical data for the Mark 2 Silicon Repeater.

<b>Dimensions:</b>	
Mask (maximum)	from 50 mm × 50 mm to 60 mm × 30 mm
Mask diagonal, maximum	70 mm
Diameter of silicon wafer	7.5, 10 or 12.5 cm (3, 4 or 5 inch)
Area of wafer movement	135 × 135 mm <sup>2</sup>
Smallest detail in projection	1.25 $\mu\text{m}$
Wavelengths for mask illumination	405 and 436 nm
Wavelength for alignment system	633 nm
<b>Time:</b>	
Exposure per projection	0.2 s
Wafer displacement (10 mm)	0.3 s
Mask-changing time (carousel)	1.5 s
Total exposure (4-inch wafer)	1 min
<b>Tolerances:</b>	
Non-parallelism of wafer	3 $\mu\text{m}/\text{cm}$
Capture range for automatic focusing	± 35 $\mu\text{m}$
Capture range of optical alignment system	88 $\mu\text{m}$
<b>Accuracy:</b>	
Max. focusing error	0.3 $\mu\text{m}$
Max. alignment error	0.08 $\mu\text{m}$
Max. positioning error	0.1 $\mu\text{m}$
Max. orthogonality error of wafer movement	0.1 arc second
Max. registration error ( <i>x</i> and <i>y</i> summed vectorially)	0.25 $\mu\text{m}$
<b>Miscellaneous:</b>	
Numerical aperture of objective	0.3
Magnification of projection optics	0.2 ×
Max. non-uniformity of exposure	2%
Number of automatically interchangeable masks	2

### Exposure of the mask

Since we wish to expose the maximum number of wafers per unit time, the exposure for each projection must be short and the luminous intensity on the wafer therefore high. In addition, to produce integrated circuits of the highest quality, the illumination of the exposed areas of the wafer must be highly uniform. This means that the mask must also be uniformly illuminated with light of the highest possible intensity.

The optical system for the exposure of the mask is shown in the upper part of fig. 2. The compact light source of the 350 W mercury lamp is located at one of the focal points of an elliptical reflector. An image of the light source is thus produced at the other focal point, which is located just in front of the integrator  $I$ . (The function of the integrator will be discussed later.) The reflector  $M_1$  is at the same time a multi-layer interference filter<sup>[4]</sup>, which only reflects radiation of wavelength less than about 450 nm and passes the rest. The reflector and the bandpass filter  $BF$ , which is also an interference filter, together ensure that more than 90% of the radiation in the wavelength range from 395 to 440 nm is transmitted. More than 95% of the radiation in the rest of the wavelength range is stopped. After spectral filtering, spatial losses

and scattering, the power of the light that reaches the integrator is only 4 W. The amount of light incident on the mask has a power of about 2 W and the wafer finally receives about 1 W of light. This power is one of the factors that determine the number of wafers that can be exposed per hour.

The operation of the integrator will be explained with reference to fig. 3. The integrator consists of a large number — 168 — of small rod lenses, whose focal length is almost the same as their physical length. The integrator and the field lens have the important task of 'smoothing out' the non-homogeneous distribution of the luminous intensity of the light-source image. The integrator also acts as a fibre-optic system with an aperture angle such that nearly all the light that reaches the second focal point of the elliptical mirror is transmitted. The lower side of the integrator can therefore be regarded as the actual light source for the projection system. An image of this 'secondary light source' is produced by the condenser in the diaphragm of the projection lens.

### Exposure of the wafer

When the photoresist is developed after exposure in the Silicon Repeater, patterns must remain that faithfully reproduce the mask pattern at a fifth of full scale. There is the problem here of interference in the transparent photoresist, between the incident light and the light reflected from the surface of the wafer. Fig. 4a-d shows what would happen if the photoresist was exposed to monochromatic light only. If there is a step in the layers of silicon oxide and aluminium originating from previous process operations (fig. 4a), the thickness of the photoresist varies at the step (fig. 4b). For a linear trace there is also a variation in the width of the positive photoresist that remains behind after development (fig. 4c), which comes about in the following way. In the ideal case the intensity of the light incident on the wafer varies with position perpendicular to the direction of the line to give a 'rectangular' pattern. However, since the optical system is not perfect, the sides of the intensity curve are not absolutely vertical. The amount of radiant energy absorbed in the photoresist varies correspondingly, but in addition it varies as a function of the film thickness (fig. 4d). The linewidth after development is therefore not the same for different film thicknesses.

We have found a solution to this problem by making simultaneous use of *two* kinds of monochromatic

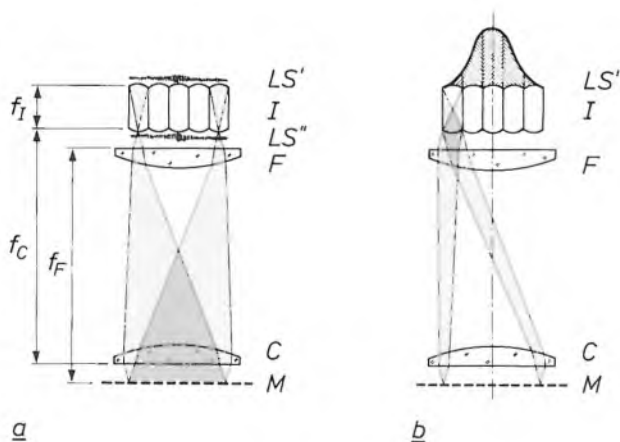


Fig. 3. Operation of the optical integrator  $I$ ; see fig. 2. (For clarity,  $M_2$  has been omitted, so that  $I$  and  $F$  are shown rotated by  $90^\circ$ .)  $I$  consists of 168 rod lenses (only five are shown) of focal length  $f_I$ . The lower and upper surfaces of the integrator are each virtually coincident with a focal plane and a principal plane of the rod lenses.  $F$  field lens of focal length  $f_F$ .  $C$  condenser lens of focal length  $f_C$ .  $M$  mask. *a*) The function of the condenser lens  $C$ . An image of the light source  $LS$  (see fig. 2) is produced as  $LS''$  just in front of the integrator. The integrator also functions as an optical-fibre system, so that the lower side of the integrator may be regarded as a 'secondary light source'  $LS''$ . The condenser  $C$  produces an image  $LS'''$  of this in the diaphragm of the projection optics (see also fig. 6). *b*) Function of the field lens  $F$ . The intensity distribution of  $LS''$  (and hence of  $LS'''$ ) is not homogeneous, as indicated diagrammatically by the bell-shaped curve at the top of the figure. With the aid of  $F$ , each rod lens spreads out the incident light over the full surface of the mask; the intensity of the incident light on one rod lens corresponds to the area of a hatched part under the bell-shaped curve. The illumination of  $M$  is therefore much more uniform than the intensity distribution of  $LS''$ .

<sup>[3]</sup> The projection optical system was designed by the firm Cerco of Paris and given the name of 'Super Tulipe'.

<sup>[4]</sup> H. Köstlin and G. Frank, Thin-film reflection filters, Philips Tech. Rev. 41, 225-238, 1983/84.

light, originating from the g and h lines of the mercury-vapour spectrum. This was achieved by means of the spectral filtering from 395 to 440 nm mentioned above. The intensity functions given in fig. 4d are

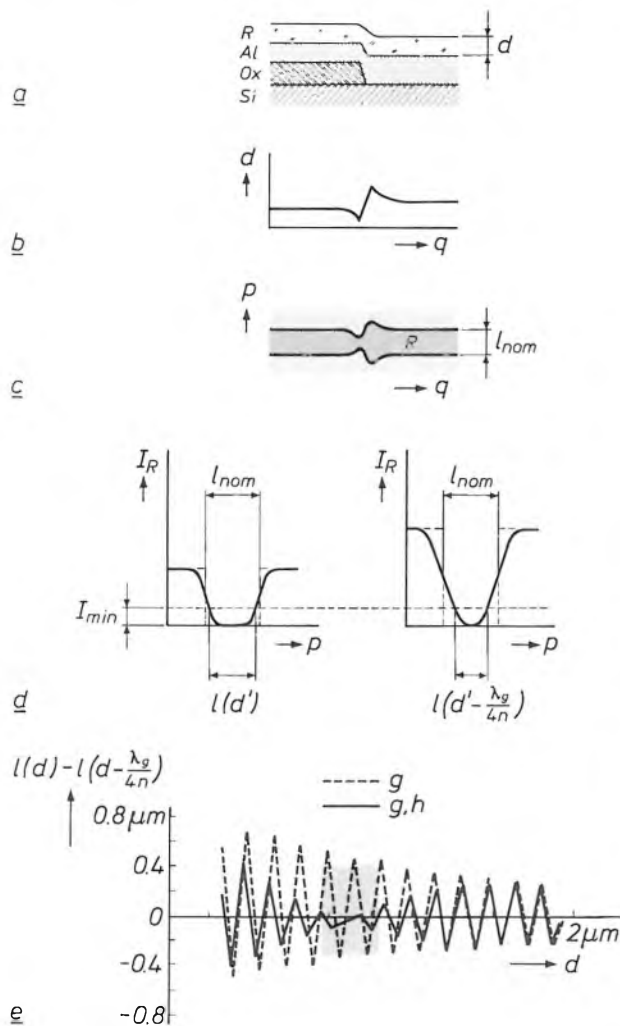


Fig. 4. Monochromatic as against bichromatic illumination of the silicon wafer. *a*) The various layers. *Si* silicon substrate, *Ox* silicon oxide, *Al* aluminium, *R* positive photoresist of thickness  $d$ . (When a positive photoresist is used the illuminated zone is removed in the development.) Because of the step in the layers *Ox* and *Al*,  $d$  is not the same everywhere. *b*) The thickness  $d$  as a function of the position  $q$ . *c*) When monochromatic illumination produces a linear track (of nominal width  $l_{nom}$ ) in *R* the linewidth varies at the position of the steps in *Ox* and *Al*. ( $p$  and  $q$  are position coordinates in the plane of the wafer.) *d*) The origin of the linewidth variation with monochromatic illumination.  $I_R$  is the light absorbed per unit area of *R* and is plotted as a function of  $p$ . The light incident on *R* does not have perfectly sharp transitions, so that the sides of the curve for  $I_R$  slope slightly and are rounded. Because of interference,  $I_R$  is also dependent on  $d$ . *Left*: The variation of  $I_R$  for a value  $d'$  of  $d$  that gives a minimum in the light absorbed. *Right*: The variation of  $I_R$  for a value  $d$  that is  $\lambda_g/4n$  smaller than  $d'$ ;  $\lambda_g$  wavelength of the monochromatic light,  $n$  the corresponding refractive index of the photoresist.  $I_{min}$  minimum light intensity necessary to dissolve *R* on development. The linewidths after development are equal to  $l(d')$  and  $l(d' - \lambda_g/4n)$ . *e*) The difference  $l(d) - l(d - \lambda_g/4n)$  as a function of  $d$  for monochromatic illumination (dashed lines) and for bichromatic illumination (continuous lines). The dashed lines have been calculated for light of the g line (436 nm), the continuous lines for light of the g and h lines (405 nm) together. With bichromatic illumination the linewidth variations partly cancel out. The range  $d = 0.9 \pm 0.15 \mu\text{m}$  in which there is little linewidth variation is shown shaded.

thus added for both wavelengths. Fig. 4e shows the beneficial effect of this bichromatic exposure<sup>[6]</sup>. (A difficulty is that a projection-lens system corrected for two wavelengths is more difficult to make than a system corrected for a single wavelength only.) With bichromatic exposure the linewidth variations approximately cancel out in a given range of film thicknesses. If we wish to limit the variation of the linewidth to  $\pm 0.1 \mu\text{m}$ , we can allow the thickness to have a spread of  $\pm 0.15 \mu\text{m}$  for a photoresist film of thickness  $0.9 \mu\text{m}$ . (In practice film thicknesses outside this range may have to be used, in which case the spread in

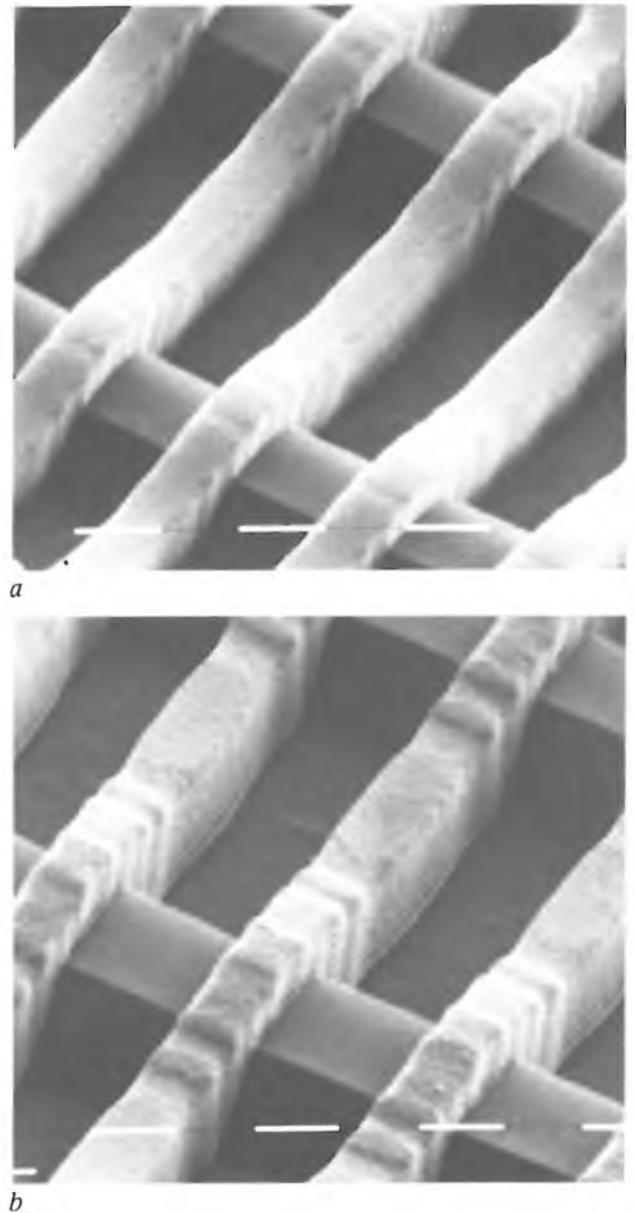


Fig. 5. Scanning electron micrographs of  $1.1\text{-}\mu\text{m}$ -wide photoresist tracks over  $1\text{-}\mu\text{m}$  steps of  $\text{SiO}_2$  in the centre of the image field *a*) for bichromatic illumination, *b*) for monochromatic illumination. In the latter case there is undesirable variation in the track width. The steep edges and uniform width of the tracks in *a* are typical of the quality of the exposure and projection optics.

linewidth will be greater and at the most equal to the variation with monochromatic exposure.)

Fig. 5 shows scanning electron micrographs of tracks of width  $1.1 \mu\text{m}$  resulting from (a) bichromatic and (b) monochromatic exposure. In case (b) the undesired variation in linewidth can clearly be seen.

#### The optical projection system

The first part of the optical projection system — the collimator — produces an image of the mask at infinity, while the second part — the objective — produces an image on the upper surface of the wafer; see fig. 6. To focus the image of the mask on the surface of the wafer it is only necessary to move the objective.

The special feature of the projection system is that both the entrance and exit pupils are located at infinity (two-sided telecentricity), so that the axes of symmetry of the light beams from the object and to the image are parallel to the optical axis. The entrance and exit pupils are both images of the diaphragm  $D$  in the common focal plane of the collimator and the objective. Fig. 6 also shows the image  $LS'''$  in  $D$  of the secondary light source  $LS''$  (see fig. 3a). This image does not completely fill the aperture of the diaphragm. The 'relative pupil filling'  $\sigma$  is defined as the ratio of the diameter of the light-source image to the diameter of the diaphragm aperture. The pupil filling determines the degree of coherence in the exposure of the wafer. With increasing  $\sigma$  the coherence decreases; when  $\sigma = 1$  the exposure is incoherent. It will be shown later that the modulation transfer function of the projection optical system depends on the coherence. Fig. 6 also shows the aperture angle  $\alpha$ , which determines the magnitude of the numerical aperture  $n \sin \alpha$  and hence — with the wavelength of the light — the resolution of the projection optics.

The collimator consists of three elements and its focal length  $f_{co}$  is 330 mm. The objective consists of thirteen elements and its focal length  $f_{ob}$  is 66 mm. The magnification is equal to the ratio  $f_{ob}/f_{co} = 0.2$ . The numerical aperture is 0.3 and the diameter of the image field is 14 mm. With this relatively small diameter, the image distortion is less than  $0.2 \mu\text{m}$ .

The imaging quality of the optical system can be evaluated by means of the modulation transfer function (MTF) [6], which gives the variation of the modulation transfer  $M$  as a function of the spatial frequency  $f$  in line pairs per mm. The shape of the MTF curve depends mainly on the wavelength, the aperture and the relative pupil filling  $\sigma$ . Fig. 7 shows some theoretical MTF curves for different values of  $\sigma$ . With increasing coherence (i.e. with decreasing  $\sigma$ ) the resolution decreases but the modulation transfer for low frequencies increases. In practice it has been

found that a modulation transfer of at least 0.6 is required to produce an image of a particular detail on the photoresist in such a way that it will not be lost after development. From fig. 7 it might therefore appear that the pupil filling  $\sigma$  ought to be as small as possible. However, the resulting high degree of coherence causes unacceptable diffraction effects ('ringing'). A good compromise is  $\sigma = 0.7$ . This value cor-

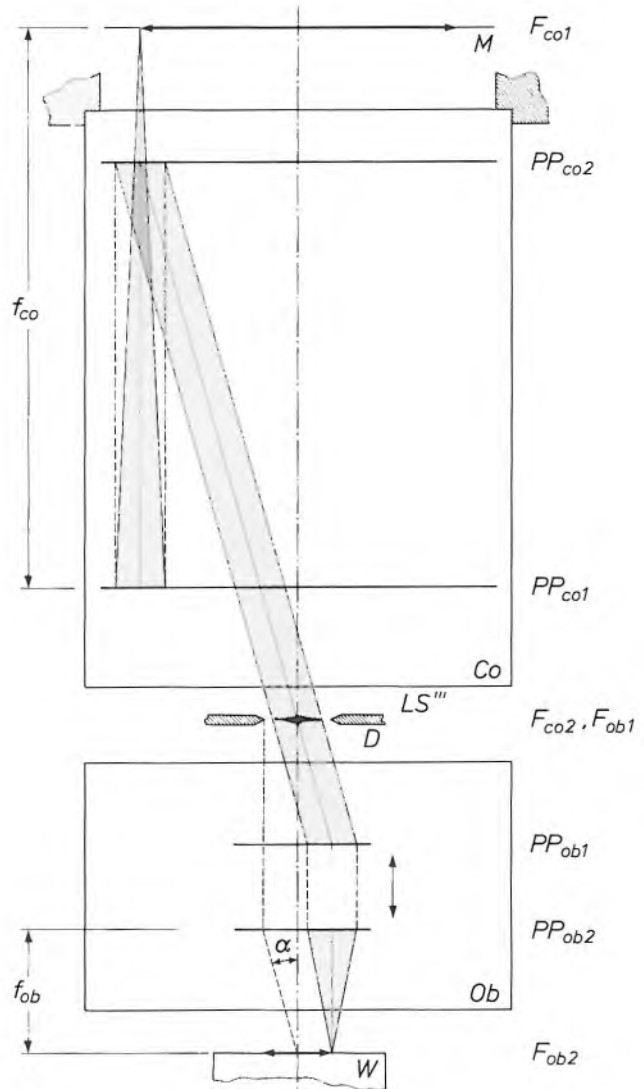


Fig. 6. Diagram of the optical projection system [3] with magnification 0.2. The optical system consists of two parts, the collimator  $Co$  and the objective  $Ob$ .  $M$  mask.  $W$  wafer.  $PP_{co1}$ ,  $PP_{co2}$ ,  $PP_{ob1}$ ,  $PP_{ob2}$  principal planes.  $F_{co1}$ ,  $F_{co2}$ ,  $F_{ob1}$ ,  $F_{ob2}$  focal planes;  $F_{co2}$  and  $F_{ob1}$  are coincident.  $f_{co}$  focal length of collimator.  $f_{ob}$  focal length of objective. The optical system is telecentric on both sides (both the entrance pupil and the exit pupil are at infinity). The entrance and exit pupils are both images of the diaphragm  $D$  in the common focal plane  $F_{co2}$ ,  $F_{ob1}$ . The image  $LS'''$  of the light source (see fig. 3a) appears at  $D$  as  $LS'''$ . Owing to the 'parallel' path of rays between  $Co$  and  $Ob$ , only  $Ob$  has to be moved for focusing, without any change in magnification. The aperture angle  $\alpha$  determines the numerical aperture, which is equal to 0.3.

[5] S. Wittekoek, Optical lithography for microcircuits, Proc. Microcircuit Engineering 80, Amsterdam 1980, pp. 155-170.  
 [6] B. van der Eijk and W. Kühl, An X-ray image intensifier with large input format, Philips Tech. Rev. 41, 137-148, 1983/84.

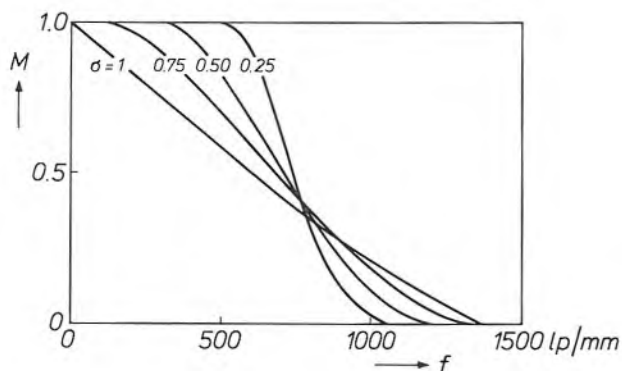


Fig. 7. The modulation transfer  $M$  of the projection optics as a function of the spatial frequency  $f$  in line pairs per mm with the relative pupil filling  $\sigma$  (the ratio of the diameters of  $LS'''$  and  $D$ , see fig. 6) as parameter. In a wafer stepper a high modulation transfer at low spatial frequencies is more important than a high resolution (the value of  $1/(2f)$  for  $M \rightarrow 0$ ).

responds to  $f \approx 600$  lp/mm at  $M = 0.6$ , so that, in favourable conditions, details of about  $0.8 \mu\text{m}$  can still be made visible in the centre of the image.

#### Focusing

After a wafer is introduced it is first clamped to the wafer table by means of gentle suction and then brought into coarse focus within  $\pm 10 \mu\text{m}$  from the image plane of the projection optics; see fig. 2. At each projection the objective section of the projection optics is then displaced in such a way that the deviation from correct focus is less than  $0.3 \mu\text{m}$  (fine focusing). This is necessary because the wafer might still not be truly flat, even though it is clamped against the flat surface of the table, and the error could increase during the process steps.

The fine focusing is done by means of an optical focusing device as illustrated in fig. 8. The light from a semiconductor laser is focused on to the wafer surface. After reflection from this surface, another image of the laser is formed on the wafer surface by a lens and reflectors. This second image of the laser is of the same size and inverted with respect to the first. Any beam asymmetry caused by the structure is therefore compensated by the double reflection on the wafer. Finally, the light beam is focused on to the photodiodes  $D_1$  and  $D_2$ . Vertical displacement of the objective lens has the effect of moving the laser image on the photodiodes.

The motor used for displacing the objective is incorporated in a control loop in which the difference between the output currents of the photodiodes is used as feedback. The displacement therefore stops when the two output currents are identical. The optics of the focusing system are arranged in such a way that the virtually constant distance between the objective and the wafer surface corresponds to the image distance.

The quality of the exposure and projection optical system described above is demonstrated by the sharp delimitation and uniform width of the tracks in fig. 5a and fig. 9.

#### Alignment of the wafer

In the successive process steps the exposed zones on the wafer must be in exact register with each other. The wafer therefore has to be brought into alignment with the mask. To make this alignment possible the wafer is provided with alignment marks before the actual process steps start. These consist of phase gratings used in reflection, which are etched into the wafer. The alignment marks on the wafer are compared with similar marks in the mask, which consist of amplitude gratings used in transmission.

The alignment marks are illustrated in fig. 10. The marks  $Gr_1$  etched into both sides of the wafer are used for the alignment of the complete wafer at the start of a series of projections for a step in the process. Each wafer has two of these alignment marks, each consisting of four separate gratings. The pitch of the two

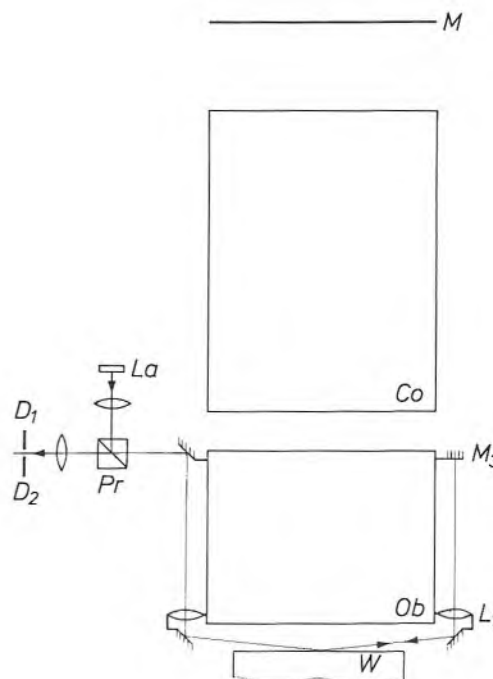


Fig. 8. The optical fine-focusing system (see also fig. 6). The light from the semiconductor laser  $La$  is focused on to the surface of the wafer  $W$  through the prism  $Pr$  with a half-silvered surface, two mirrors and two lenses. The light is reflected from  $W$  to form another image of  $La$  on  $W$  by means of a mirror, the lens  $L_1$  and a mirror  $M_3$ . Mirror  $M_3$  and the intersection point of the rays with  $W$  are located at the focal planes of  $L_1$ . After the second reflection from  $W$ , a final image of  $La$  is formed on the photodiodes  $D_1$  and  $D_2$ . The difference signal produced by  $D_1$  and  $D_2$  is used for controlling the focusing motor ( $FM$  in fig. 2) for the vertical movement of the objective  $Ob$ .

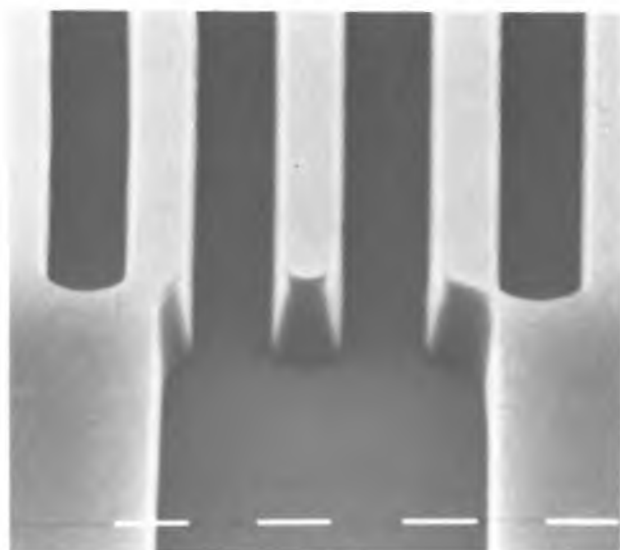


Fig. 9. Scanning electron micrograph demonstrating the quality of the exposure and projection optics. Photoresist tracks are shown with a width of  $1.2 \mu\text{m}$  and a thickness of  $1.2 \mu\text{m}$  on a silicon-oxide film with a thickness of  $0.3 \mu\text{m}$ .

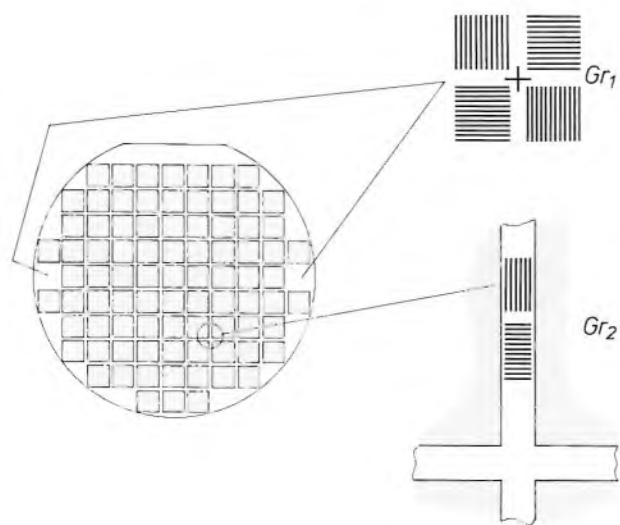


Fig. 10. The alignment marks consisting of phase gratings applied to the 'virgin' wafer. The marks  $Gr_1$  serve for aligning the wafer in relation to the mask at the start of a series of projections. There are two alignment marks  $Gr_1$ , each consisting of four gratings, applied to opposite sides of the wafer. The two left-hand gratings of  $Gr_1$  have a pitch of  $16 \mu\text{m}$ , the two right-hand gratings a pitch of  $17.6 \mu\text{m}$ . The dimensions of  $Gr_1$  are  $400 \mu\text{m}$  by  $400 \mu\text{m}$ . The alignment marks  $Gr_2$  serve for alignment at each projection and are mainly used when the wafer has nonlinear deformation. For each projection zone (shown shaded) there is one alignment mark  $Gr_2$  consisting of two gratings. The gratings of  $Gr_2$  have a pitch of  $16 \mu\text{m}$ . The dimensions of  $Gr_2$  are  $80 \mu\text{m}$  by  $400 \mu\text{m}$ .

gratings on the left is  $16 \mu\text{m}$ , that of the two on the right is  $17.6 \mu\text{m}$ .

The marks  $Gr_2$  are only  $80 \mu\text{m}$  wide. They are located between the projection areas (shaded), which are intended for the actual circuits on the wafer. These gratings are used for realignment before each projection. Each projection zone has an alignment mark

$Gr_2$ , consisting of two separate gratings. The pitch of these gratings is  $16 \mu\text{m}$ .

When a wafer is introduced into the Silicon Repeater the wafer table is displaced in such a way that the two marks  $Gr_1$  on the wafer coincide in turn with a mark on the mask. The computer in the wafer stepper then calculates, from the measured coordinates of each mark, the origin for the displacements and the angle that the line through the two marks makes with the  $x$ -direction of the table movement. The wafer is then rotated through this angle.

If a nonlinear deformation of the wafer is suspected, the marks  $Gr_2$  can be used to align the wafer for each projection. The marks  $Gr_2$  can also be used when the Silicon Repeater is used with a 1:1 projector in IC manufacture ('mix-and-match' procedure). A 1:1 projector as mentioned in the introduction can be used for the process steps that do not require such high accuracy. The processing time for a wafer can then be reduced. When a 1:1 projector is used the gratings are applied to the wafer with this projector at the start of production. Deviations due to image distortion produced by this projector are then recorded on the wafer by the positions of the marks  $Gr_2$ . When these marks are used for aligning the wafer at each projection in the Silicon Repeater, the quality of the integrated circuit is almost unaffected by errors due to the 1:1 projector.

The alignment system is illustrated in *fig. 11a*<sup>[7]</sup>. One of the alignment gratings on the wafer  $W$  is illuminated through a prism by a helium-neon laser at a wavelength of  $633 \text{ nm}$ . The reflected radiation is diffracted by the grating. In diffraction, light is reflected only at an angle of  $\theta_k$  to the normal to the grating surface and in a plane perpendicular to the grating lines, where  $\sin \theta_k = k\lambda/p$ ;  $k$  is the order and  $\lambda$  the wavelength of the reflected light, and  $p$  is the pitch of the grating. In the common focal plane of collimator and objective there is an order diaphragm, made from material that transmits the light for illuminating the wafer but not the light from the helium-neon laser. The order diaphragm has holes in it at locations such that light of order  $k = 1$  and  $k = -1$  reflected from the grating at a wavelength of  $633 \text{ nm}$  is transmitted; see *fig. 11b*. This light is then incident on the mask. Here, as a result of interference, a periodic pattern is again formed with a pitch 2.5 times greater than that of the grating on the wafer. The position of the mask does indeed correspond to a five-fold magnification, but only the images of the second harmonics (with  $k = 1$  and  $k = -1$ ) of the gratings are formed on the

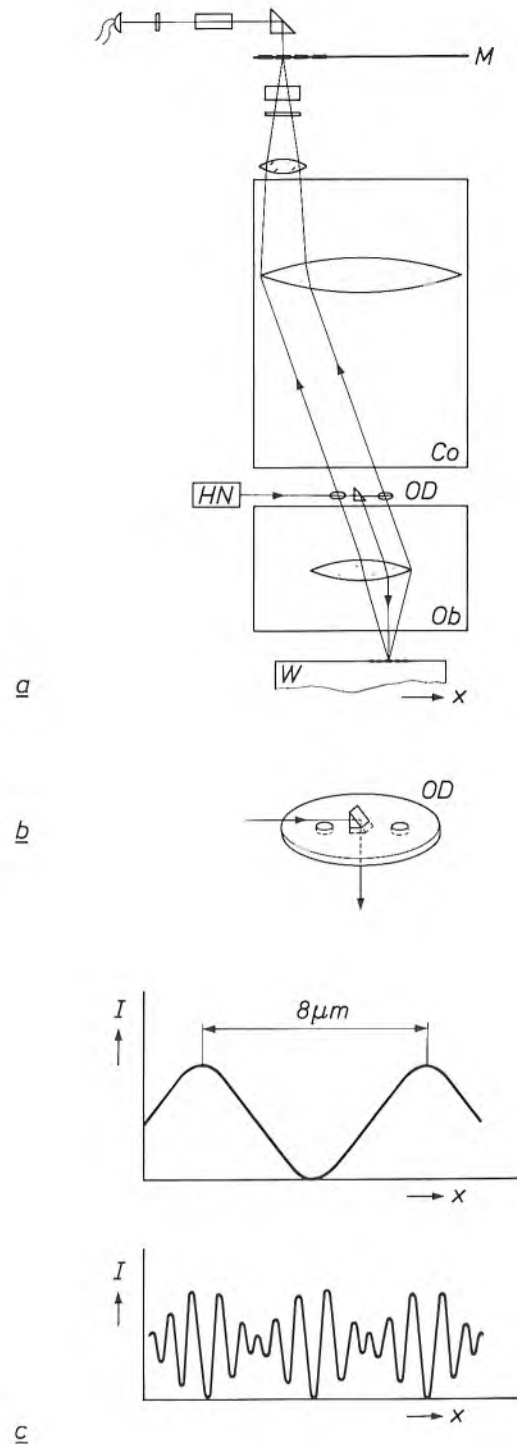
[7] G. Bouwhuis and S. Wittekoek, Automatic alignment system for optical projection printing, IEEE Trans. ED-26, 723-728, 1979.

**Fig. 11.** The optics of the alignment system. *a)* A reflection phase grating on the wafer  $W$  is illuminated through the lower prism by a helium-neon laser  $HN$  with a wavelength of 633 nm. The projection optics produces an image of this grating on a corresponding transmission amplitude grating on the mask  $M$ . The gratings lie with their lines perpendicular to the plane of the drawing, so that alignment can take place in the  $x$ -direction. The order diaphragm  $OD$ , which is located at the common focal plane  $F_{co2}$ ,  $F_{ob1}$  (see fig. 6), transmits the light for illuminating the wafer but stops most of the 633-nm light. The operation of the other components of the alignment system is explained in fig. 12. *b)* The order diaphragm  $OD$  and the lower prism, shown in perspective and on a rather larger scale. The material of the diaphragm has two holes for alignment in the  $x$ -direction (there are two other holes, not shown, for alignment in the  $y$ -direction), which transmit only the light of order 1 and  $-1$  at a wavelength of 633 nm. *c)* When the intensity  $I$  of the 633-nm light transmitted through the grating on the mask is measured as a function of the wafer displacement  $x$ , the curve shown in the upper part of the figure is obtained. Its spatial period is  $8\ \mu\text{m}$  if the gratings on the wafer and mask with pitches of 16 and  $40\ \mu\text{m}$  coincide. The upper signal is sensitive to electrical interference and the maximum or minimum cannot easily be detected. To get around this difficulty, the signal is modulated at a frequency of 50 kHz, as indicated in the lower figure (for a constant wafer velocity). This modulation is explained in fig. 12.

wafer, resulting in a doubling of the spatial frequency. Assuming that the  $16\text{-}\mu\text{m}$  grating of the alignment mark  $Gr_1$  is observed, then the corresponding grating on the mask must have a pitch of  $40\ \mu\text{m}$ . A measurement of the intensity of light  $I$  at a wavelength of 633 nm that is transmitted through the grating surface in  $M$  would show that this varies with a spatial period of  $8\ \mu\text{m}$  when the wafer is displaced; see fig. 11c, above. In principle this can be used for aligning the wafer in relation to the mask. In such a case, however, the wafer must not be more than  $\pm 4\ \mu\text{m}$  from the correct position, and the accuracy with which the position of the minimum or the maximum of the periodic signal can be detected is not particularly high. The alignment accuracy can be increased by modulating the output signal from the alignment system by a signal at a fixed frequency, as illustrated in fig. 11c, below. This will now be explained, and also a method for increasing the capture range of the alignment system.

#### Signal processing in the alignment system

The detection system is illustrated in detail in fig. 12a, which also indicates the function of the various optical elements. Before the light at a wavelength of 633 nm reaches the mask, it first passes through a polarizer and a birefringent crystal. In this way the light is first linearly polarized and then split into two beams whose planes of polarization are rotated through  $-45^\circ$  and  $+45^\circ$ . The beams are also displaced relatively by half the pitch of the grating (i.e. by  $20\ \mu\text{m}$ ). The light then passes through the mask and an optical modulator. This consists of a quartz crystal to which a 50-kHz alternating voltage  $V_{ref}$  is applied in such a way that the polarization plane of the light is rotated by  $-45^\circ$  during the positive part of



$V_{ref}$  and by  $+45^\circ$  during the negative part of  $V_{ref}$ . The light next passes through an analyser that has the same principal direction as the polarizer. Finally the light reaches a detector. The electronic signal from the detector is amplified and then processed in a phase-sensitive detector, to which  $V_{ref}$  is also applied.

Fig. 12b shows the operations performed on the light in the various optical elements, on the left for positive  $V_{ref}$  and on the right for negative  $V_{ref}$ . Fig. 12c indicates the electronic processing performed on the signal from the detector at three different places in the

circuit and for three different positions of the wafer. Because the output signal is modulated by the alternating voltage  $V_{ref}$  the phase-sensitive detector responds strongly to variations in alignment. In this way variations down to  $0.02 \mu\text{m}$  can be detected. The out-

put signal is also much less sensitive to electrical interference and variations in the optical transmission or the supply voltage.

If the alignment system were actually designed in the manner described above, the alignment field would

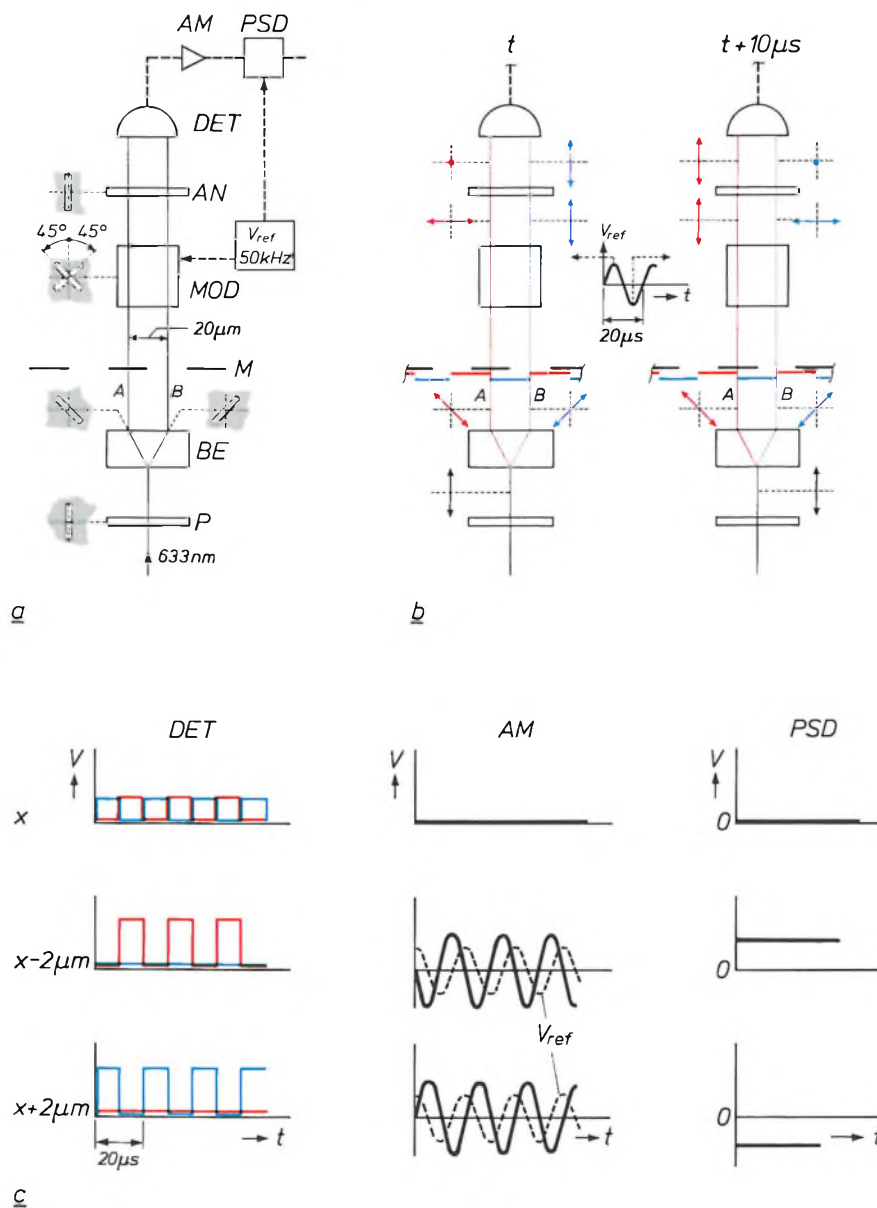


Fig. 12. Signal detection in the alignment system. *a*) The various optical and electronic components, and the effect of the optical components on the state of polarization of the 633-nm laser light. *P* polarizer. *BE* birefringent crystal, splitting the light into beams *A* and *B* (shown as lines) with plane of polarization rotated  $-45^\circ$  and  $+45^\circ$ , and displaced  $-10 \mu\text{m}$  and  $+10 \mu\text{m}$ .  $V_{ref}$  50-kHz alternating voltage. *MOD* optical modulator: periodic rotation of the plane of polarization by  $-45^\circ$  (during positive  $V_{ref}$ ) and  $+45^\circ$  (during negative  $V_{ref}$ ). *AN* analyser. *DET* optical detector, which produces a direct voltage proportional to the light intensity. *AM* alternating-voltage amplifier. *PSD* phase-sensitive detector. *b*) Effect of the optical components on the beams *A* (red) and *B* (blue) during positive (left) and negative (right)  $V_{ref}$ . The position of the wafer is such that the beam-*A* and beam-*B* images of the wafer grating are displaced  $10 \mu\text{m}$  to the left and  $10 \mu\text{m}$  to the right in relation to the mask grating. In this position *DET* therefore only receives a signal from beam *B* on the left and only receives a signal from beam *A* on the right. *c*) The electronic signals after *DET* (left-hand column), after *AM* (centre column) and after *PSD* (right-hand column). In the upper row the wafer is in the position  $x$  (as in *b*); in the centre row it is in the position  $x - 2 \mu\text{m}$ , and in the lower row in the position  $x + 2 \mu\text{m}$ . (The square-wave voltage after *DET* is in reality sinusoidal; see fig. 11c.) The alternating voltages produced at positions  $x - 2 \mu\text{m}$  and  $x + 2 \mu\text{m}$  by *AM* are shifted in phase by  $-90^\circ$  and  $+90^\circ$  with respect to  $V_{ref}$ . Since *PSD* responds both to amplitude differences and to phase differences, *PSD* produces a direct voltage that is highly sensitive to small displacements of the wafer.

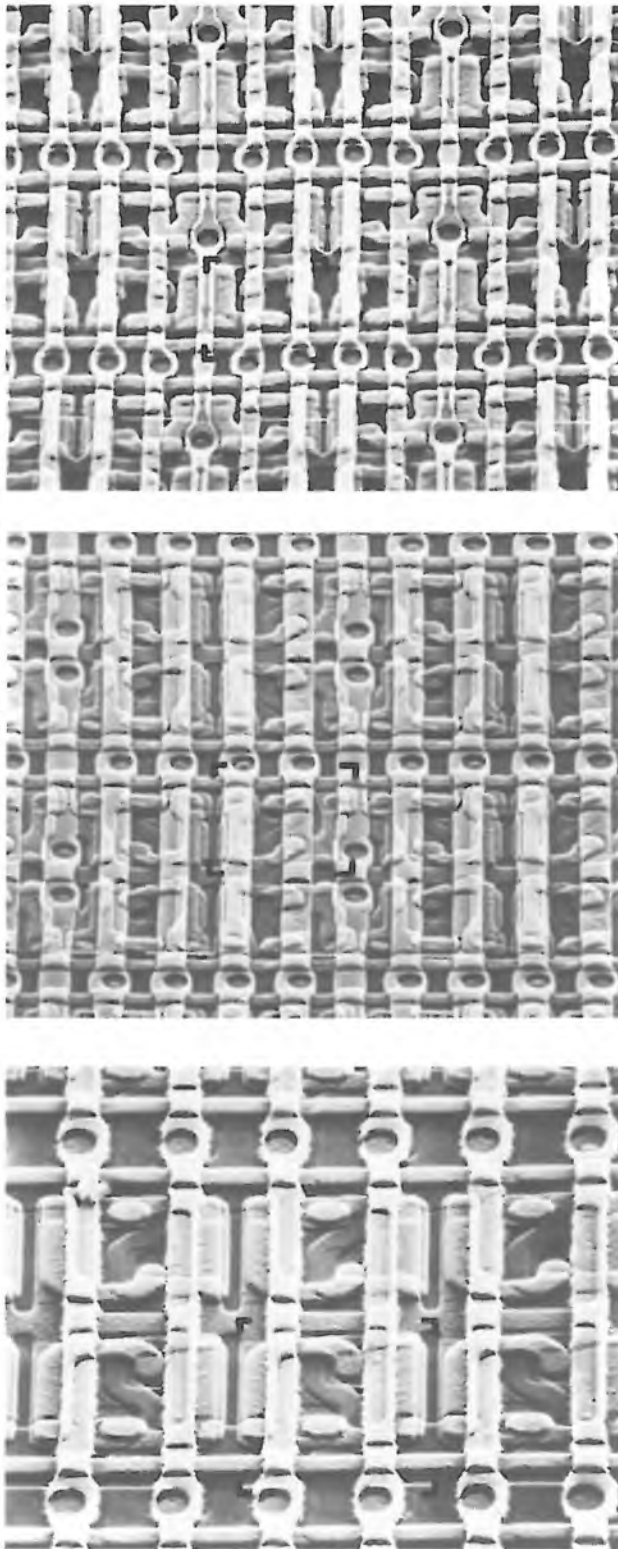


Fig. 13. Scanning electron micrographs of 16-K memory circuits of the static-RAM type (random-access memory) in NMOS technology. In each micrograph the corners of a memory cell are indicated. From bottom to top the dimensions of a cell are  $28 \mu\text{m}$  by  $38 \mu\text{m}$ ,  $21 \mu\text{m}$  by  $28.5 \mu\text{m}$  and  $17.5 \mu\text{m}$  by  $21 \mu\text{m}$ . (The dimensions quoted first are measured horizontally in the photograph.) The increase in packing density of the circuits was achieved by process improvements and mainly by using the Silicon Repeater for the upper circuit. The centre and lower circuits were both made with the aid of a 1:1 projector. In the circuits 'pits' are visible, for making contact between the aluminium tracks running from top to bottom of the photograph and the underlying diffusion layers. The pits in the upper circuit are clearly much more accurately centred with respect to the tracks. This is due to the high alignment accuracy of the Silicon Repeater.

$40 \mu\text{m}$  and the gratings of pitch  $17.6$  and  $44 \mu\text{m}$  can be measured at the same time. The capture range of the alignment system is considerably widened by taking the simultaneous production of a minimum in the output signal of both detector systems as the alignment criterion (rather like a vernier). The coincidence of the two minima is repeated with a periodicity of  $8(8 + 0.8)/0.8 = 88 \mu\text{m}$  in the displacement of the wafer. The capture range of the alignment system is thus increased 11 times, and is sufficient for the use of automatic wafer feed with mechanical pre-alignment.

Fig. 13 shows that the packing density of a memory circuit can be considerably increased by using the Silicon Repeater in its fabrication. The circuit shown in the upper part of the figure was made with this wafer stepper, the two others with a 1:1 projector. The upper picture clearly shows that the depositions made in the successive process steps are in much more exact register because of the highly advanced alignment system of the Silicon Repeater.

The development of the Silicon Repeater was the work of a group of research workers, in particular of H. J. Bartelings (electronics and software), A. G. Bouwer (mechanical design), T. Fahner (focusing system), G. C. van de Looij (exposure), R. H. Munnig Schmidt (servosystems) and J. E. van der Werf (alignment system). The author of this article was responsible for coordinating the development project.

be very small. It has already been mentioned that the pitches of the two left-hand gratings of  $G_{r1}$  in fig. 10 are equal to  $16 \mu\text{m}$  and those of the two right-hand gratings to  $17.6 \mu\text{m}$ , resulting in pitches of  $40$  and  $44 \mu\text{m}$  for the corresponding gratings on the mask. The detector  $DET$  has four quadrants, so that the degree of overlap between the gratings of pitch  $16$  and

**Summary.** With the Silicon Repeater sixty 4-inch silicon wafers for integrated circuits can be exposed per hour. This high production rate is possible because of the high intensity and the high efficacy of the illumination from a 350-W high-pressure mercury-vapour lamp with an elliptical reflector. The illumination of the mask is highly uniform, partly through the use of an optical integrator. Linewidth variations due to interference in the photoresist are largely avoided by using light at two wavelengths ( $405$  and  $436 \text{ nm}$ ). Image details of  $1.25 \mu\text{m}$  can be produced, through the use of a specially designed two-sided telecentric projection system with high resolution, and because the repeater has a focusing system that reduces focusing errors to  $0.3 \mu\text{m}$  or less. An alignment system ensures that the exposures for the successive steps of the process are in accurate register. This system uses phase gratings on the wafer, which are brought into register with amplitude gratings on the mask. Alignment errors as small as  $0.02 \mu\text{m}$  can be detected.

## Scientific publications

These publications are contributed by staff of laboratories and plants that form part of or cooperate with enterprises of the Philips group of companies, particularly by staff of the research laboratories mentioned below. The publications are listed alphabetically by journal title.

Philips GmbH Forschungslaboratorium Aachen, Weißhausstraße, 5100 Aachen, Germany	A
Philips Research Laboratory Brussels, 2 avenue Van Becelaere, 1170 Brussels, Belgium	B
Philips Natuurkundig Laboratorium, Postbus 80 000, 5600 JA Eindhoven, The Netherlands	E
Philips GmbH Forschungslaboratorium Hamburg, Vogt-Kölln-Straße 30, 2000 Hamburg 54, Germany	H
Laboratoires d'Electronique et de Physique Appliquée, 3 avenue Descartes, 94450 Limeil-Brévannes, France	L
Philips Laboratories, N.A.P.C., 345 Scarborough Road, Briarcliff Manor, N.Y. 10510, U.S.A.	N
Philips Research Laboratories, Cross Oak Lane, Redhill, Surrey RH1 5HA, England	R
Philips Research Laboratories Sunnyvale P.O. Box 9052, Sunnyvale, CA 94086, U.S.A.	S

C. Ronse	B	A three-stage construction for multi-connection networks	Acta Inf. 20	197-206	1983
M. Auphan	L	Réponse impulsionnelle des sphères molles ou rigides	Acustica 54	50-51	1983
P. van Dooren	B	Reducing subspaces: computational aspects and applications in linear system theory	Analysis and optimization of systems, A. Bensoussan & J. L. Lions (eds), Springer, Berlin	935-953	1982
K. H. J. Buschow	E	Some fundamental and technological aspects of research on rare-earth base metal systems	Ann. Meeting Rare Earth Soc. Japan, Osaka 1983	15-37	1983
P. van de Weijer & R. M. M. Cremers	E	Hook method: improvement and simplification of the experimental setup	Appl. Opt. 22	3500-3502	1983
J. A. van Steenwijk	E	Correct relation between the impulse response of GRIN fibers and the excitation by a laser diode	Appl. Opt. 22	3864-3868	1983
J. J. Harris, D. E. Ashenford (GEC Hirst Res. Centre, Wembley), C. T. Foxon, P. J. Dobson (Imp. College, London) & B. A. Joyce	R	Kinetic limitations to surface segregation during MBE growth of III-V compounds: Sn in GaAs	Appl. Phys. A 33	87-92	1984
M. Erman & P. M. Frijlink	L	Interface analysis by spectroscopic ellipsometry of Ga <sub>1-x</sub> Al <sub>x</sub> As-GaAs heterojunctions grown by metal organic vapor phase epitaxy	Appl. Phys. Lett. 43	285-287	1983
M. Erman, N. Vodjdani, J. B. Theeten & J. P. Cabanié	L	Low loss waveguides grown on GaAs using localized vapor phase epitaxy	Appl. Phys. Lett. 43	894-895	1983
H. Rau, H. A. Friedrichs* & W. Mathia* (* RWTH, Aachen)	A	p-V-T and bubble-point measurements in the system HBr-H <sub>2</sub> O and its critical behaviour	Ber. Bunsenges. Phys. Chem. 87	1181-1187	1983
V. Belevitch	B	On the anti-sidetone telephone circuit	Circuits Syst. & Signal Process. 2	99-117	1983
J. L. W. Kessels	E	On-the-fly optimization of data structures	Commun. ACM 26	895-901	1983
R. Memming	H	Processes at semiconductor electrodes	Comprehensive treatise of electrochemistry, Vol. 7, B. E. Conway et al. (eds), Plenum, New York	529-592	1983
C. Tsironis & D. Hennings	L, A	Highly stable FET DROs using new linear dielectric resonator material	Electronics Lett. 19	741-743	1983

- P. Bachmann, P. Geittner, H. Hübner, D. Leers & M. Lennartz *A* Material dispersion characteristics of optical fibres prepared by the PCVD process *Electronics Lett.* **19** 765-767 1983
- L. Fortuin (*Philips ISA-CQM, Eindhoven*) Initial supply and re-order level of new service parts *Eur. J. Oper. Res.* **15** 310-319 1984
- A. Shaulov & W. A. Smith *N* Optimum cuts of monoclinic m crystals for pyroelectric detectors *Ferroelectrics* **49** 223-228 1983
- A. M. van der Kraan (*Interuniv. Reactor Inst., Delft*), K. H. J. Buschow & T. T. M. Palstra (*Univ. Leiden*) *E* Magnetic behaviour of the cubic La(Fe,Al)<sub>13</sub> compounds *Hyperfine Interactions* **15/16** 717-720 1983
- C. A. A. J. Greebe, L. J. van de Polder & S. L. Tan *E* Consumer displays for hi-fi television *IBA Tech. Rev. No. 21* 42-45 1983
- A. R. Cusdin & N. C. W. Fane (*RSRE, Great Malvern*) *R* Performance of an interferometer angle-measuring receiver against non line-of-sight transmitters *IEE Proc.* **130** 695-700 1983
- J. W. Slotboom, M. J. J. Theunissen & A. J. R. de Kock *E* Impact of silicon substrates on leakage currents *IEEE Electron Device Lett.* **EDL-4** 403-406 1983
- J. L. van Meerbergen & F. J. van Wijk *E* A 256-point discrete Fourier transform processor fabricated in a 2 μm NMOS technology *IEEE J. SC-18* 604-609 1983
- V. Pauker & M. Binet *L* Wideband high gain small size monolithic GaAs FET amplifiers *IEEE MTT-S Int. Microwave Symp. Digest, Boston 1983* 50-53 1983
- P. Röschmann & K. M. Lüdeke *H* A ferrimagnetic resonance sensor for remote wireless temperature measurements in organic tissue *IEEE MTT-S Int. Microwave Symp. Digest, Boston 1983* 192-194 1983
- C. Tsironis, R. Stahlmann (*Tech. Univ. Aachen*) & R. Meierer *L* Modelling and evaluation of dual gate MESFETs as low-noise, self-oscillating and image-rejection mixers *IEEE MTT-S Int. Microwave Symp. Digest, Boston 1983* 443-445 1983
- S. Shokoohi (*Bell Labs, Holmdel, NJ*), L. M. Silverman (*Univ. Los Angeles*) & P. M. van Dooren *B* Linear time-variable systems: balancing and model reduction *IEEE Trans. AC-28* 810-822 1983
- M. H. Kuhn & H. H. Tomaschewski *H* Improvements in isolated word recognition *IEEE Trans. ASSP-31* 157-167 1983
- Y. Kamp & C. J. Wellekens *B* Optimal design of minimum-phase FIR filters *IEEE Trans. ASSP-31* 922-926 1983
- T. A. C. M. Claasen & W. F. G. Mecklenbräuker (*Techn. Univ. Wien*) *E* The aliasing problem in discrete-time Wigner distributions *IEEE Trans. ASSP-31* 1067-1072 1983
- M. Lemonier & C. Piaget *L* Characterization of local transfer defects in CCD's using a multireversal transfer mode *IEEE Trans. ED-30* 1414-1416 1983
- A. Broese van Groenou & M. I. L. Uijterschout *E* A quick test on wear of head materials by recording tapes *IEEE Trans. MAG-19* 1674-1676 1983
- W. F. Druyvesteyn, L. Postma, G. H. J. Somers & J. de Wilde *E* Thin-film read head for analog audio application *IEEE Trans. MAG-19* 1748-1750 1983
- R. L. Maresca *N* An integrated magnetic actuator and sensor for use in linear or rotary magnetic bearings *IEEE Trans. MAG-19* 2094-2096 1983
- C. Tsironis & V. Pauker *L* Temperature stabilization of GaAs MESFET oscillators using dielectric resonators *IEEE Trans. MTT-31* 312-314 1983
- A. J. M. Houtsma (*Inst. Perception Res., Eindhoven*) Estimation of mutual information from limited experimental data *J. Acoust. Soc. Am.* **74** 1626-1629 1983
- M. T. M. Scheffers (*Inst. Perception Res., Eindhoven*) Simulation of auditory analysis of pitch: An elaboration on the DWS pitch meter *J. Acoust. Soc. Am.* **74** 1716-1725 1983
- A. Broese van Groenou & R. C. D. Lissenburg *E* Inhomogeneous density in die compaction: experiments and finite-element calculations *J. Am. Ceram. Soc.* **66** C/156-C/158 1983
- F. Evers (*Hermal-Chemie, Hamburg*), K. Kobs, R. Memming & D. R. Terrell (*Agfa-Gevaert, Mortsel*) *H* Intramolecular excimer emission of poly(*N*-vinylcabazole) and *rac*- and *meso*-2,4-Di-*N*-carbazolylpentane. Model substances for its syndiotactic and isotactic dyads *J. Am. Chem. Soc.* **105** 5988-5995 1983
- D. J. Breed, P. Q. J. Nederpel & W. de Geus *E* Domain-wall dynamics in garnet films with orthorhombic anisotropy *J. Appl. Phys.* **54** 6577-6583 1983
- S. C. Abrahams\*, R. Liminga\*, P. Marsh\* (\* *Bell Labs, Murray Hill, NJ*) & G. M. Loiacono *N* Strontium nitrite monohydrate: A new pyroelectric nonlinear optic material *J. Appl. Phys.* **54** 6776-6778 1983

- G. J. van Gorp, A. H. van Ommen, P. R. Boudewijn, D. P. Oosthoek & M. F. C. Willemsen *E* Ion implantation and diffusion of Zn in GaAs *J. Appl. Phys.* **55** 338-346 1984
- J. Hasker *E* Comment on 'A study of cathode edge emission' *J. Appl. Phys.* **55** 792-793 1984
- J. W. D. Martens, W. L. Peeters, P. Q. J. Nederpel & M. Erman *E, L* Polar magneto-optical Kerr effect and the dielectric tensor elements of  $\text{CoFe}_{2-x}\text{Al}_x\text{O}_4$   $0.1 < x < 1$  in the photon energy range  $0.65 < h\nu < 4.5$  eV *J. Appl. Phys.* **55** 1100-1104 1984
- M. Zijlstra (*Philips ISA-CQM, Eindhoven*) Characterizations of the geometric distribution by distributional properties *J. Appl. Prob.* **20** 843-850 1983
- M. Duseaux *L* Temperature profile and thermal stress calculations in GaAs crystals growing from the melt *J. Cryst. Growth* **61** 576-590 1983
- C. Belouet\*, C. Texier-Hervo\*, M. Mautref\* (\* *CGE, Marcoussis*), C. Belin, J. Paulin & J. Schneider *L* Growth of polysilicon sheets on a carbon shaper by the RAD process *J. Cryst. Growth* **61** 615-628 1983
- R. B. Heimann (*McMaster Univ., Hamilton, Canada*) & W. Tolksdorf *H* Dissolution forms of gadolinium gallium garnet and yttrium iron garnet obtained in lead oxide/boron trioxide flux *J. Cryst. Growth* **62** 75-86 1983
- L. de Jonge (*Philips ISA-CQM, Eindhoven*) & W. M. Oppedijk van Veen (*Univ. Tilburg*) Accounting for data inconsistencies in a longitudinal mail survey *J. Econ. Psychol.* **4** 377-400 1983
- W. A. P. Claassen, W. G. J. N. Valkenburg, F. H. P. M. Habraken (*Univ. Utrecht*) & Y. Tamminga *E* Characterization of plasma silicon nitride layers *J. Electrochem. Soc.* **130** 2419-2423 1983
- A. van Eenbergen & E. Bruninx *E* A study of some instrument characteristics of an LHS-10 electron spectrometer *J. Electron Spectrosc. & Rel. Phenom.* **33** 51-60 1984
- J. B. Clegg, J. B. Mullin (*RSRE, Malvern*), K. J. Timmins (*MQAD, Royal Arsenal East, London*), G. W. Blackmore (*Admiralty Mater. Technol. Est., Poole*), G. L. Everett (*Johnson & Matthey Chem. Ltd, Royston*) & R. Snook (*Imp. College, London*) *R* Measurement of impurities in a multi-doped sample of cadmium mercury telluride *J. Electronics Mater.* **12** 879-889 1983
- J. J. Daniele & A. Lewis *N* Electroepitaxial (Peltier-induced) liquid phase epitaxy, compositional stabilization and X-ray analysis of thick (120  $\mu\text{m}$ )  $\text{In}_{1-x}\text{Ga}_x\text{P}$  epilayers on (100) GaAs *J. Electronics Mater.* **12** 1015-1031 1983
- K. H. J. Buschow & D. B. de Mooij *E* Note on the crystal structure of  $\text{EuGa}_2$  *J. Less-Common Met.* **97** L5-L8 1984
- K. H. J. Buschow *E* Magnetic properties of  $\text{Y}_2\text{Ni}_7$  and its hydride *J. Less-Common Met.* **97** 185-190 1984
- P. C. Scholten *E* How magnetic can a magnetic fluid be? *J. Magn. & Magn. Mater.* **39** 99-106 1983
- K. H. J. Buschow *E* Magnetic properties of  $\text{La}_2\text{Ni}_7$  and its hydride *J. Magn. & Magn. Mater.* **40** 224-226 1983
- K. H. J. Buschow, P. G. van Engen & D. B. de Mooij *E* Magnetic and magneto-optical properties of Heusler alloys of the type  $\text{Ni}_3-x\text{Mn}_x\text{Sn}$  *J. Magn. & Magn. Mater.* **40** 339-347 1984
- G. de With *E* High temperature fracture of boron carbide: experiments and simple theoretical models *J. Mater. Sci.* **19** 457-466 1984
- K. M. Lüdeke & J. Köhler *H* Microwave radiometric system for biomedical 'true temperature' and emissivity measurements *J. Microwave Power* **18** 277-283 1983
- D. M. Krol & J. G. van Lierop *E* The densification of monolithic gels *J. Non-Cryst. Solids* **63** 131-144 1984
- B. J. Mulder *E* Simple piezoelectric microbalance based on a vibrating quartz wire *J. Phys. E* **17** 119-121 1984
- P. C. M. Gubbens\*, A. M. van der Kraan\* (\* *Interuniv. Reactor Inst., Delft*) & K. H. J. Buschow *E* Magnetic interactions in  $\text{Tm}_6\text{Fe}_{23}$  and its hydride as studied by means of  $^{169}\text{Tm}$  and  $^{57}\text{Fe}$  Mössbauer spectroscopy *J. Phys. F* **14** 235-243 1984
- K. H. J. Buschow *E* Short-range order and thermal stability in amorphous alloys *J. Phys. F* **14** 593-607 1984

M. Duseaux, C. Schiller, J. P. Cornier, J. P. Chevalier (C.N.R.S., Vitry-sur-Seine) & J. Hallais	L	Elimination of dislocations in GaAs single crystals	J. Physique 44 (Colloque C4)	C4/397- C4/407	1983
M. Erman, J. B. Theeten, N. Vodjdani & Y. Demay	L	Chemical and structural analysis of the GaAs/AlGaAs heterojunctions by spectroscopic ellipsometry	J. Vac. Sci. & Technol. B 1	328-333	1983
J. Maluenda & P. M. Frijlink	L	Abrupt transitions in composition and doping profile in GaAs-Ga <sub>1-x</sub> Al <sub>x</sub> As heterostructures by atmospheric pressure MOVPE	J. Vac. Sci. & Technol. B 1	334-337	1983
K. H. Nicholas, R. A. Ford, H. E. Brockman & I. J. Stemp	R	The magnitude and significance of proximity effects in electron image projector defined layers	J. Vac. Sci. & Technol. B 1	1020-1022	1983
A. A. van Gorkum	E	Correction of spherical aberration in charged particle lenses using aspherical foils	J. Vac. Sci. & Technol. B 1	1312-1315	1983
Y. Genin, P. van Dooren, T. Kailath*, J.-M. Delosme* & M. Morf* (* Stanford Univ., CA)	B	On $\Sigma$ -lossless transfer functions and related questions	Linear Algebra & Appl. 50	251-275	1983
P. van Dooren & P. Dewilde (Univ. of Technol., Delft)	B	The eigenstructure of an arbitrary polynomial matrix: computational aspects	Linear Algebra & Appl. 50	545-579	1983
P. Delsartre, Y. Genin & Y. Kamp	B	On the Toeplitz embedding of an arbitrary matrix	Linear Algebra & Appl. 51	97-119	1983
H. Dötsch, D. Mateika, P. Röschmann & W. Tolksdorf	H	Growth and properties of epitaxial barium hexaferrite films	Mater. Res. Bull. 18	1209-1216	1983
E. D. Roberts & C. E. Fuller	R	A positive-working cross-linked electron resist with improved resistance to plasma-etching processes	Microcircuit Engineering 83	297-304	1983
P. Willich, A. P. von Rosenstiel* & N. Drost* (* TNO, Apeldoorn)	H	Quantitative electron probe microanalysis of sputtered FeC dry lubrication films	Mikrochim. Acta Suppl. 10	211-216	1983
Y. Tamminga, M. F. C. Willemsen & R. van Silfhout	E	Optimization and application of glancing angle Rutherford backscattering spectrometry	Nucl. Instrum. & Methods Phys. Res. 218	107-110	1983
W. J. Dallas & R. Linde	H	X-ray coded-aperture image reconstruction using an array of kinoforms	Opt. Acta 30	1561-1572	1983
P. A. Devijver & M. Dekesel	B	Computing multidimensional Delaunay tessellations	Pattern Recognition Lett. 1	311-316	1983
H. K. Kuiken	E	An analysis of the temperature drop across a double-layered medium	Philips J. Res. 38	273-294	1983
D. Hennings & P. Schnabel	A	Dielectric characterization of Ba <sub>2</sub> Ti <sub>9</sub> O <sub>20</sub> type ceramics at microwave frequencies	Philips J. Res. 38	295-311	1983
R. Knöchel, K. M. Lüdeke & W. Meyer	H	Mikroellen in der Medizin	Phys. Bl. 39	337-342	1983
P. Hansen & K. Witter	H	Magneto-optical properties of gallium-substituted yttrium iron garnets	Phys. Rev. B 27	1498-1506	1983
P. Hansen, K. Witter & W. Tolksdorf	H	Magnetic and magneto-optic properties of lead- and bismuth-substituted yttrium iron garnet films	Phys. Rev. B 27	6608-6625	1983
B. H. Verbeek, H. W. A. M. Rompa, P. K. Larsen, M. S. Methfessel* & F. M. Mueller* (* Univ. Nijmegen)	E	Mixed states in RhAl, RhGa, and RhIn studied by photoemission spectroscopy and band-structure calculations	Phys. Rev. B 28	6774-6779	1983
P. Dawson, G. Duggan, H. I. Ralph & K. Woodbridge	R	Free excitons in room-temperature photoluminescence of GaAs-Al <sub>x</sub> Ga <sub>1-x</sub> As multiple quantum wells	Phys. Rev. B 28	7381-7383	1983
P. M. T. M. van Attekum, P. H. Woerlee, G. C. Verkade & A. A. M. Hoeben	E	Influence of grain boundaries and surface Debye temperature on the electrical resistance of thin gold films	Phys. Rev. B 29	645-650	1984
G. F. Neumark	N	Pair spectra and evaluation of the dielectric constant: Application to ZnSe	Phys. Rev. B 29	1050-1051	1984
M. M. Broer*, D. L. Huber*, W. M. Yen* (* Univ. Wisconsin, Madison, WI) & W. K. Zwicker	N	Fluorescence quenching and spectral diffusion in La <sub>1-x</sub> P <sub>5</sub> O <sub>14</sub> :Nd <sub>x</sub> <sup>3+</sup>	Phys. Rev. B 29	2382-2389	1984
G. F. Weston	R	Developments in high-vacuum pumps	Phys. Technol. 15	37-44	1984
M. F. H. Schuurmans & J. M. F. van Dijk	E	On radiative and non-radiative decay times in the weak coupling limit	Physica 123B	131-155	1984

F. A. Vollenbroek, E. J. Spiertz & H. J. J. Kroon	E	Profile modification of resist patterns in optical lithography	Polym. Eng. & Sci. 23	925-930	1983
E. D. Roberts	R	A dry-etch resistant positive-working electron resist	Polym. Eng. & Sci. 23	968-974	1983
B. Sastra & G. M. Dohmen	E	High-precision numerically-controlled measuring system for cylindrical surfaces	Precision Eng. 6	12-16	1984
M. Davio, J.-P. Deschamps & A. Thayse	A, B	Machines algorithmiques	Presses Polytechniques Romandes, Lausanne	—	1983
M. H. Kuhn & R. Geppert	H	Performance criteria and the role of integrated circuit technology for voice input systems	Proc. Conf. on communications equipment and systems, Birmingham 1982	80-86	1982
P. J. Severin	E	Chromatic launching, a new method for optical fibre profile, single-mode, and mode-dependent measurements	Proc. 9th ECOC, Genève 1983	185-188	1983
P. B. Hesdahl*, A. M. J. Koonen* & M. Weeda* (* Philips' Telecommun. Ind., Huizen)		A multi service single fibre subscriber network with wideband electro-optical switching	Proc. 9th ECOC, Genève 1983	331-334	1983
G. D. Khoe, J. A. Luijendijk & A. C. Jacobs	E	Application of UV-excited fluorescence for the preparation of single mode fibre connectors and splices	Proc. 9th ECOC, Genève 1983	413-416	1983
J. van der Heijden	E	Fibre optic broadband multiservice networks	Proc. 9th ECOC (invited & post deadline papers), Genève 1983	8 pp.	1983
H. Baudry & G. Kersuzan ( <i>T.R.T., Le Plessis Robinson</i> )	L	Individual encapsulation for integrated circuits: how to use thermal analysis to optimize curing conditions towards reliability	Proc. 4th Eur. Hybrid Microelectronics Conf., Copenhagen 1983	111-121	1983
M. Monneraye, H. Baudry & D. Bri-cout ( <i>RTC, Evreux</i> )	L	The adhesion of thick-film copper conductors	Proc. 4th Eur. Hybrid Microelectronics Conf., Copenhagen 1983	240-249	1983
P. Frey, B. Gabillard & M. Rocchi	L	Subnanosecond 8 bit normally-off GaAs SRAM	Proc. ESSCIRC'83, Lausanne 1983	65-68	1983
H. Dötsch, G. Martens & W. Meyer	H	Fibre optic components for industrial control	Proc. First Int. Conf. on Optical fibre sensors, London 1983	67-71	1983
B. Aldefeld	H	Automatic 3D reconstruction from 2D geometric part descriptions	Proc. IEEE Comput. Soc. Conf. on Computer vision and pattern recognition, Washington, D.C., 1983	66-72	1983
G. M. Martin, M. Duseaux & J. P. Farges	L	Characterization of GaAs and InP crystals for integrated optics	Proc. 4th Int. Conf. on Integrated optics and optical fiber communication, Kobe 1983	13-16	1983
H. Ney	H	Dynamic programming as a technique for pattern recognition	Proc. 6th Int. Conf. on Pattern recognition, München 1982	1119-1125	1982
H. K. Kuiken	E	Etching: a two-dimensional mathematical approach	Proc. R. Soc. London A 392	199-225	1984
E. Lindale & D. Lehrfeld ( <i>Magnavox, Mahwah, NJ</i> )	N	Life test performance of a Philips rhombic-drive refrigerator with bellows seals	Proc. SPIE 364	103-108	1983
R. Ward, A. R. Franklin, P. Gould, M. J. Plummer & I. H. Lewin	R	Prospects for the 1:1 electron image projector	Proc. SPIE 393	233-239	1983
J. Braat	E	Aspherical lenses in optical scanning systems	Proc. SPIE 399	294-298	1983
A. T. Entoff	N	Improved Philips Air Sandwich Disk	Proc. SPIE 420	150-159	1983
R. H. Coursant, C. Méquio & P. Pesqué	L	Simulation of the acousto-electric response of ultrasonic narrow strip transducers with mechanical losses	Proc. Ultrasonics International 83, Halifax 1983	414-419	1983
H. W. Werner & R. P. H. Garten ( <i>Inst. Spektrochem. &amp; angew. Spektrosk., Dortmund</i> )	E	A comparative study of methods for thin-film and surface analysis	Rep. Progr. Phys. 47	221-344	1984

C. Alibert*, F. J. Hua* (* Univ. Sci. & Tech. Languedoc, Montpellier), M. Erman, P. Frijlink, P. Jarry & J. B. Theeten	L	Electroréflexion et ellipsométrie spectroscopique d'hétérostructures InGaAsP/InP et GaAlAs/GaAs	Revue Phys. Appl. 18	709-717	1983
P. Delsarte, Y. Genin & Y. Kamp	B	Equivalence classes of Hermitian matrices and their Schur parametrization	SIAM J. Algebraic & Discrete Methods 4	279-289	1983
A. J. E. M. Janssen	E	A note on Hudson's theorem about functions with nonnegative Wigner distributions	SIAM J. Math. Anal. 15	170-176	1984
H. Strecker	H	A local feature method for the detection of flaws in automated X-ray inspection of castings	Signal Process. 5	423-431	1983
C. R. Hill	N	A real-time microprocessor debugging technique	SIGPLAN Not. 18 (No. 8)	145-148	1983
M. Barthelmes, P. Bressler, D. Bünz, K. Gütschow, J. Heeger & H.-J. Lemke	H	CATPAC: a software package for computer-aided control engineering	Simulation in engineering sciences, J. Burger & Y. Jarny (eds), Elsevier Science, Amsterdam	73-78	1983
J. Hallais	L	Metal organic vapour phase epitaxy: the key issues	Solid state devices 1982, A. Goetzberger & H. M. Zerbst (eds), Verlag Chemie, Weinheim	51-72	1983
M. J. Sparnaay & G. E. Thomas	E	Surface segregation in Au <sub>0.1</sub> Cu <sub>0.9</sub> crystals	Surf. Sci. 135	184-198	1983
J. W. D. Martens, W. L. Peeters & P. Q. J. Nederpel	E	A non-destructive analysis of the influence of sputter etching on the magnetic surface properties of manganese zinc ferrite	Surf. Sci. 135	334-340	1983
M. Erman & J. B. Theeten	L	Analysis of ion-implanted GaAs by spectroscopic ellipsometry	Surf. Sci. 135	353-373	1983
J. van der Heijden	E	Het DIVAC project	T. Ned. Elektron. & Radiogenoot. 48	171-177	1983
R. L. J. Roetering (Philips' Telecommun. Ind., Huizen)		A/D-conversie van video-signalen en lijncodering	T. Ned. Elektron. & Radiogenoot. 48	189-199	1983
S. Gourrier, P. Friedel & J. P. Chané	L	Interface properties of metal/oxide/semiconductor and metal/insulator/semiconductor structures on Ga <sub>1-x</sub> In <sub>x</sub> As with x = 0.35 and 0.10	Thin Solid Films 103	155-166	1983
M. Fink, F. Hottier & J. F. Cardoso	L	Ultrasonic signal processing for <i>in vivo</i> attenuation measurement: short time Fourier analysis	Ultrason. Imaging 5	117-135	1983
H. W. Werner & P. R. Boudewijn	E	A comparison of SIMS with other techniques based on ion-beam solid interactions	Vacuum 34	83-101	1984
J. M. Shannon & J. B. Clegg	R	Nanometre structures in semiconductors formed by low energy ion implantation	Vacuum 34	193-197	1984
A. J. van Roosmalen	E	Review: dry etching of silicon oxide	Vacuum 34	429-436	1984
R. Memming	H	Photoelektrochemische Wasserstoff-Erzeugung durch Solarenergie	Wärme 89	62-66	1983

Contents of Philips Telecommunication Review 42, No. 2, 1984

Q. Renni & J. R. Lange: PFX, a new universal portable (pp. 49-62)

A. Brinkman & A. L. Bloemendaal: A motorway traffic control system (pp. 63-73)

A. J. W. van Daal & P. van der Vlist: DELTACS — a versatile tactical communications system (pp. 74-89)

W. J. A. Vonk: AEROPP 0 message and data switch for smaller airports (pp. 90-94)

P. G. L. Potgieser: The LAM91/95 family of data circuit terminating equipments (pp. 95-105)



J. van der Heijden: DIVAC — an experimental optical-fibre communications network,  
Philips Tech. Rev. **41**, 253-259, 1983/84 (No. 9).

The DIVAC project has resulted in an experimental optical-fibre communications network, which connects an exchange with two 'subscribers'. Five organizations have participated in this trial project, with the object of gaining experience with new technologies and assessing the reactions of potential users and bodies. Various digital signals, for telephony, audio, video and broadband services can be carried simultaneously and in two directions by means of TDM, WDM and FDM on a pair of optical fibres for each subscriber. The various services made available include selection television. The subscriber uses this to operate a switching network to select the required service: broadcast television, local television, a video library or pay television. The video library contains a collection of LaserVision discs, and has a control computer, a number of LaserVision players and a mechanical retrieval and transport system.

S. Wittekoek: Optical aspects of the Silicon Repeater,  
Philips Tech. Rev. **41**, 268-278, 1983/84 (No. 9).

With the Silicon Repeater sixty 4-inch silicon wafers for integrated circuits can be exposed per hour. This high production rate is possible because of the high intensity and the high efficacy of the illumination from a 350-W high-pressure mercury-vapour lamp with an elliptical reflector. The illumination of the mask is highly uniform, partly through the use of an optical integrator. Linewidth variations due to interference in the photoresist are largely avoided by using light at two wavelengths (405 and 436 nm). Image details of 1.25  $\mu\text{m}$  can be produced, through the use of a specially designed two-sided telecentric projection system with high resolution, and because the repeater has a focusing system that reduces focusing errors to 0.3  $\mu\text{m}$  or less. An alignment system ensures that the exposures for the successive steps of the process are in accurate register. This system uses phase gratings on the wafer, which are brought into register with amplitude gratings on the mask. Alignment errors as small as 0.02  $\mu\text{m}$  can be detected.

H. F. Huisman and C. J. F. M. Rasenberg: Porosimeter measurements on magnetic tape,  
Philips Tech. Rev. **41**, 260-266, 1983/84 (No. 9).

With a commercial mercury porosimeter, modified in various ways to give higher sensitivity, measurements can be made of the pore volume, the total pore area and the pore-volume distribution of magnetic tape. In calculating the results the curve giving the change in mercury volume as a function of mercury pressure has to be corrected for the compressibility of the mercury and the change in the volume of the dilatometer. The total pore area and the pore distribution are obtained by integration and differentiation of the corrected curve. From pore-volume measurements on different tape samples the critical pigment concentration can be determined. If this concentration is exceeded, pores are formed, but this negative effect can be eliminated by calendaring.

